MASTER

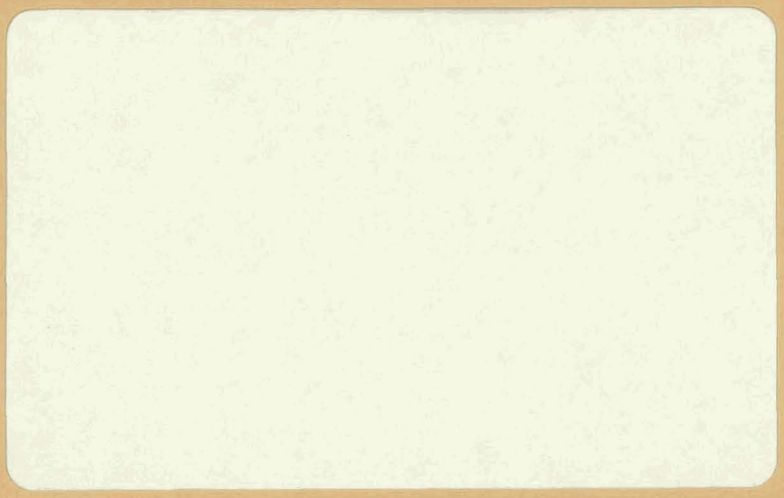

JAYCOR

Post Office Box 370
1401 Camino Del Mar
Del Mar, California 92014

DISCLAIMER

JAYCOR

JAYCOR Report No. J510-80-015/2184

MICROWAVE HEATING OF THE ELMO BUMPY TORUS RELATIVISTIC ELECTRON RING

Status Report for period covering

November 1, 1979 - September 30, 1980

Prepared by

S. Hamasaki, H. H. Klein, N. A. Krall,
J. B. McBride* and J. L. Sperling

Prepared for

U. S. Department of Energy
Office of Fusion Energy
Washington, D. C. 20545

DOE Contract No. DE-AC03-80ER53092

October 1980

*Present address: SAI, La Jolla, CA, 92037

EXECUTIVE SUMMARY

This manuscript is a final report giving the technical output of JAYCOR's scientists under DOE Contract No. DE-AC03-80ER53092, entitled "Theoretical Studies of Energetic Electron Rings in EBT." During the eleven month period covering the duration of the contract, JAYCOR, as directed by DOE, formulated a relativistically correct model for the electron cyclotron resonance heating of EBT rings. This model has been used to calculate both the steady state ring temperature and ring power requirements through the balancing of heating rate against existing models for energy loss.

The first section of the report is an introduction describing the critical importance of the relativistic electron rings to the EBT concept and the significance of electron-cyclotron heating to the formation and steady state of the rings. The relation and distinctive features of the present work to previous calculations of ring power balance are delineated.

In the second section of the report the plasma model used as the basis of the calculations is set up. Special emphasis is given to the development and description of a relativistically correct quasilinear expression. Equations for collisional, synchrotron radiation and bremsstrahlung losses which are necessary for determining steady state annulus temperatures are written down. In the heating and loss formulas, the ring momentum distribution function is assumed to be the relativistic Maxwellian.

In the third section the energy loss and quasilinear heating equations are adapted to EBT geometry. The wave properties necessary to complete the quasilinear description of the ring heating are noted. The relativistic quasilinear equation is then averaged over magnetic lines. The result is a distinctive expression not used in previous ring power balance calculations.

The fourth section gives a detailed accounting of spatial locations where quasilinear heating occurs for various electron cyclotron harmonics. The equations for field line averaged quasilinear heating and energy loss are evaluated and the results are carefully explained in order to determine steady state ring temperatures under different assumptions for wave propagation. It

is shown that annulus steady state temperature is very sensitive to the assumptions made about wave propagation and amplitude characteristics. Ring power requirements at the steady state are determined and shown to be consistent with previous calculations. The significance of fundamental electron-cyclotron heating in ring start-up is noted and carefully analyzed.

The final section makes concluding remarks about the JAYCOR EBT ring model. A brief synopsis is given of the significant points deduced from the model, particularly as they relate to recent EBT experiments. Based on the results, suggestions for future refinements in the JAYCOR ring model are made which can permit improvement in the theoretical description of the EBT ring.

ABSTRACT

A model for microwave heating of electron rings in the ELMO Bumpy Torus configuration is analyzed using a relativistically correct quasilinear formulation. The steady state ring energy and the microwave power required to sustain the rings are determined by balancing the line averaged heating rate against classical collisional and radiative energy loss processes. Electron-cyclotron resonances, especially the first and second, contribute to ring heating at steady state. It is shown that fundamental electron-cyclotron heating by extraordinary waves could account for initial ring formation. The model predicts ring power requirements for EBT-1 which are consistent with previous estimates.

TABLE OF CONTENTS

I. INTRODUCTION

The ELMO Bumpy Torus (EBT) confinement concept[1] consists of a toroidally linked set of simple mirror sections. A central element in this concept is the presense of high beta electron annuli formed in the mirror sections by microwave electron cyclotron resonance heating (ECRH) on appropriate surfaces of constant magnetic field. The annuli enclose a toroidal core plasma and are of sufficient density and temperature that the associated diamagnetic currents modify the vacuum magnetic field so as to provide MHD stability against otherwise unstable interchange modes. Both theoretical and experimental studies have shown that stable high beta annuli can be formed[2-8] and stabilize a toroidal plasma.

Microwave electron-cyclotron resonance heating of fusion oriented devices (e.g., bumpy tori and tokamaks) is an area of present experimental and theoretical investigation.[9-11] To a large extent the present interest is motivated by the continued and encouraging development of efficient microwave sources of the gyrotron type.[12-14] Furthermore, microwaves have sufficiently short wavelengths that wave propagation characteristics can be accurately predicted by ray tracing techniques. Because microwaves are not as susceptible to nonlinear effects as some other wave heating methods (e.g., lower-hybrid heating), spatial locations where microwave absorption occur are readily predicted from linear considerations.[9] This property of microwave heating makes it a prime candidate for controlling current and temperature profiles in fusion oriented devices. However, whereas microwave heating is only an auxiliary heating method in other plasma configurations, it is a necessary ingredient for maintaining stable bumpy torus plasmas.

Because of the importance of electron-cyclotron resonance heating in the attractive bumpy torus reactor concept,[15,16] we have undertaken a quantitative calculation of the heating in the geometry, parameter ranges and mode structure of bumpy torus experiments. In this work, the heating rate by ECRH and cooling rates by radiation and collisional drag are calculated for a hot electron population imbedded in a background plasma with fixed density and temperature. Like previous calculations, relativistically correct expressions are

used for the radiative and collisional losses which determine whether the electrons cool or heat.[17,18] The distinctive feature of the present work is the use of a relativistically correct quasilinear (velocity space) diffusion model which allows a reliable calculation of ECR heating rates at high temperatures, and at various cyclotron harmonics, including the important effect of relativistic broadening of the cyclotron frequency, $\Omega = \Omega_0\sqrt{1 - v^2/c^2}$, as well as possible nonlinear heating effects.

Subsequent portions of this paper are divided in the following way. In the second section, the plasma model used to determine the heating rate of a distribution of relativistic electrons by microwaves of fixed frequency ω_0 in a given magnetic field is described. Section III discusses the adaptation of the model to EBT geometry and microwave source. Application of the model to heating by the two polarizations, which are normal modes of a cold plasma, extraordinary and ordinary waves, are presented in Section IV. In the final section we make concluding remarks relating to our calculations and directions for future work. Three appendices cover details pertinent to the calculations.

II. PLASMA MODEL FOR CALCULATIONS

In this section we focus on a systematic determination and understanding of the electron cyclotron resonance heating process, calculating a relativistically correct heating rate for first, second and higher harmonic heating and for both ordinary and extraordinary wave polarization. Collisional drag with the background is calculated for the same parameters. This work extends earlier work[17,18] by formulating a relativistically correct microwave heating rate based on the quasilinear interaction of the electrons with the microwave electric fields. By balancing this expression for power input against the existing expressions for the classical energy loss processes, a self-consistent determination of many of the properties of the hot electron annulus in EBT may be possible.

The quasilinear approach has been employed in a different but analogous situation by Stix[19] to treat ion cyclotron heating in tokamaks. Since the ring particles reach quite high kinetic energies, on the order of the electron rest mass, a relativistic description of the heating process is necessary. Using the relativistic Vlasov equation, the familiar results of nonrelativistic quasilinear theory[20] are generalized in a straightforward way by making the following replacements:

$$\underset{\sim}{k} \longrightarrow \underset{\sim}{k}/m_o\gamma$$

$$\underset{\sim}{v} \longrightarrow \underset{\sim}{p}$$

$$\Omega_o \equiv eB_o/m_oc \longrightarrow \Omega = \Omega_o/\gamma$$

$$e \longrightarrow em_o$$

where $p = \gamma m_o \underset{\sim}{v}$ and $\gamma = (1 + p^2/m_o^2c^2)^{\frac{1}{2}}$. The result is:

$$\frac{\partial f_o(p_\perp, p_z)}{\partial t} = \frac{\pi}{2}\left(\frac{e}{\omega}\right)^2 \sum_k \sum_n \left[\frac{1}{p_\perp}\frac{\partial}{\partial p_\perp} n\Omega + \frac{\partial}{\partial p_z}\frac{k_z}{m_o\gamma}\right] |\theta|^2$$

$$\delta\left(\omega - n\Omega - \frac{k_z p_z}{m_o\gamma}\right) \cdot \left[\frac{n\Omega}{p_\perp}\frac{\partial}{\partial p_\perp} + \frac{k_z}{m_o\gamma}\frac{\partial}{\partial p_z}\right]$$

$$f_o\ (p_\perp, p_z) \qquad (1)$$

where

$$\theta \equiv p_\perp\ E_-\ J_{n-1}\ (b)\ e^{i\psi} + p_\perp\ E_+\ J_{n+1}(b)\ e^{-i\psi} + (2)^{\frac{1}{2}}\ p_z E_z J_n(b)$$

$$\underset{\sim}{k} = \hat{e}_x\ k_\perp\ \cos\ \psi + \hat{e}_y\ k\ \ \sin\ \psi + \hat{e}_z\ k_z$$

$$b \equiv k_\perp\ p_\perp / m_o\ \Omega_o$$

and f_o is the solution to the (zeroth order) Vlasov equation. The symbol $\perp$ means perpendicular to the magnetic field, $\underset{\sim}{B}_o$, and the z- direction is chosen to lie along $\underset{\sim}{B}_o$. The left-hand and right-hand circularly polarized wave electric fields are denoted by E_+ and E_-, respectively. The z-directed electric field is written as E_z.

To define the problem, we assume that the annulus distribution function can be represented as a tail on the bulk electron distribution. Specifically, the form of the tail we have chosen is the relativistic Maxwellian:

$$f_o\ (p_\perp, p_z) = \frac{(m_o c^2/T)}{4\pi\ (m_o c)^3\ K_2\ (m_o c^2/T_A)} \exp\left[-\frac{m_o c^2}{T_A}(\gamma - 1)\right] \qquad (2)$$

where K_2 is the modified Bessel function of the second kind and order two. This choice of distribution function permits the electron heating rate by waves to be written as:

$$\frac{dW}{dt} \equiv \int d^3p\, \gamma m_o c^2 \frac{\partial f_o(p_\perp, p_z)}{\partial t}$$

$$= \frac{\pi}{4} \frac{\omega_{pA}^2}{m_o T_A} \sum_k \sum_n \int p_\perp\, dp_\perp \int dp_z\, \gamma^{-2}\, \delta(\omega - n\Omega - k_z p_z/m_o\gamma)$$

$$|\theta|^2\, f_o(p_\perp, p_z) \qquad (3)$$

where

$$\omega_{pA}^2 = \frac{4\pi n_A e^2}{m_o} \qquad (4)$$

is annulus plasma frequency for density n_A and rest mass m_o.

Eq. (3) includes the resonance condition (in the δ-functions), the relstivistic mass shift which shifts the location of cyclotron resonance at high energies, the polarization (E_+, E_-, E_z), and harmonic contributions through the Bessel function, $J_n(b)$.

To calculate the steady state annulus temperature, the heating rate, dW/dt, must be balanced against loss mechanism acting to reduce the energy of the relativistic electrons. As in Refs. 17 and 18, only classical loss mechanisms are considered. For an infinite and homogeneous plasma:

$$\frac{dW}{dt} = P_{sync} + P_{brems} + P_{coll} \quad . \qquad (5)$$

The terms on the right hand side of the equation are the powers per unit volume lost from the ring due to synchrotron radiation, bremsstrahlung, and collisions with the background plasma, respectively. Specifically,

$$P_{sync} = 6.2 \times 10^{-21}\, B_o^2\, n_A T_A\, (1 + T_A/2.04 \times 10^5)\ \text{ergs/cm}^3\text{-sec} \qquad (6a)$$

$$P_{brems} = 1.5 \times 10^{-25}\, n_A n_o T_A^{\frac{1}{2}}\, (1 + T_A/m_o c^2)$$

$$\left[3 - \frac{2}{(1 + T_A/m_o c^2)^2}\right]\ \text{ergs/cm}^3\text{-sec} \qquad (6b)$$

$$P_{coll} = 80\pi\, n_A n_o\, e^4 \int d^3p\, \frac{\gamma}{p}\, f_o(p_\perp, p_z) \qquad (6c)$$

where magnetic fields (B), densities (n) and energy (T, $m_o c^2$) are in units of gauss, cm^{-3}, and eV, respectively. The background density is represented by n_o. Eq. (6a) is taken from Ref. 21. The expression in Eq. (6b), from Ref. 22, includes both electron-electron as well as electron-ion bremsstrahlung, since both contributions become of comparable importance as electrons become relativistic. The relativistically correct form of Eq. (6c) found in Ref. 23, assumes a Coulomb logarithm value of twenty.

III. ADAPTATION TO EBT GEOMETRIES

Because the rates of heating and cooling depend [Eq. (3)] on wave amplitude, wave polarization, and cyclotron frequency (a function of v and B), a number of details of the magnetic and microwave structure for a particular experiment must be included in applying the model.

A fundamental question is the spatial distribution of microwave energy, including the general question of whether the microwaves emitted from the antennas will penetrate to the region where they could cause resonant heating. It is assumed that the propagation characteristics of the microwaves in EBT are determined by the cold background plasma. Annulus effects on propagation are neglected. This is consistent with the absorption lengths calculated in this paper. Under such circumstances two modes of propagation, ordinary and extraordinary, exist in the plasma.[10,24] The cold plasma dispersion relation in the electron-cyclotron frequency range gives the cutoff condition (i.e., index of refraction going to zero) for the ordinary mode:

$$\omega_{pe}^2 = \omega^2 \quad , \tag{7}$$

and for the extraordinary mode:

$$\omega_{pe}^2 = \omega^2 (1 - \Omega_o/\omega) \quad . \tag{8}$$

The symbol ω_{pe} denotes the bulk electron plasma frequency. Furthermore, the extraordinary mode has a resonance (i.e., index of going to infinity) at:

$$\omega_{pe}^2 = \omega^2 (\omega^2 - \Omega_o^2)/[\omega^2 - \Omega_o^2 k_z^2/(k_z^2 + k_\perp^2)] \quad . \tag{9}$$

Extraordinary waves are also strongly absorbed in cold plasmas at spatial locations where:

$$\omega \approx \Omega_o \tag{10}$$

because of the large right-hand circularly polarized component of the wave electric field. However, the ordinary wave does not have an appreciable right-hand circularly polarization and therefore is unaffected by propagation across spatial locations where Eq. (10) is satisfied.

Figure 1, taken from Ref. 10, contains a sketch of the resonance and cutoff regions in EBT.

The right-hand cutoff condition of Eq. (8) indicates that an extraordinary wave propagating from the low magnetic field and low density region will never reach the first harmonic heating resonance, $\omega = \Omega_o$, for a finite (non-zero) density plasma. This implies that heating by an extraordinary wave propagating directly from outside in EBT is only possible for higher harmonics than the first harmonic resonance. However, the ordinary mode propagates for all densities such that:

$$\omega_{pe}^2 \leq \omega^2 \qquad (11)$$

and so conversion of ordinary to extraordinary waves could permit extraordinary wave energy to exist at all spatial locations where extraordinary wave propagation is allowed, even in the bumpy torus throat with wave frequencies less than the local nonrelativistic electron-cyclotron frequency. One powerful conversion mechanism is the reflection of ordinary waves off the conducting walls of the bumpy torus. Such conversion is a necessary consequence of the boundary conditions for Maxwell's equations at a conducting surface. In Appendix A and Ref. 10 substantial conversion efficiencies in excess of ten percent are predicted for wave propagation which is oblique to the magnetic field.

With the existence of extraordinary wave energy in the mirror throat, a mechanism for startup of a hot electron annulus can be conjectured. With the microwave frequency equal to the second harmonic of the nonrelativistic electron-cyclotron frequency near the annulus location the microwave frequency is equal to the fundamental of the electron-cyclotron frequency away from the midplane and nearer to the throat of each mirror section (see Figure 1). Because fundamental electron heating will be shown to be effective for electrons of zero energy, cold electrons can increase their momentum and energy in the direction

perpendicular to the magnetic field. Eventually the perpendicular energy gets sufficiently large that the second and higher harmonic resonance heating can increase the electron energy to the relativistic level appropriate to the steady state EBT annulus. Details of a calculation showing how fundamental heating can increase the energy electrons in the early stage of annulus formation are described in Appendix B.

Finally, the heating rate depends on the magnetic geometry (Ω_o compared to the microwave frequency). We use the following analytic form for the magnetic field strength:

$$B_z(r,z') = 0.5\, B_o \left[3 - I_o \left(\frac{\pi}{L} r\right) \cos \left(\frac{\pi}{L} z'\right)\right]$$

$$B_r(r,z') = 0.5\, B_o\, I_1 \left(\frac{\pi}{L} r\right) \sin \left(\frac{\pi}{L} z'\right)$$

where I_o is the modified Bessel function, r the mirror radius, and z' the axial location relative to z' = 0 at the midplane of the mirror. Device parameters are L = 19.64 cm and B_o = 4500 gauss for EBT-1 and 7000 gauss for EBT-S. This form for the fields is appropriate to a straight cylinder and assumes that only vacuum magnetic fields are present. Hence, plasma diamagnetism is neglected.

Using this magnetic field, the quasilinear heating rate expression can then be averaged over a field line to obtain an average heating rate for a distribution of electrons in an EBT geometry:

$$\left\langle \frac{dW}{dt} \right\rangle = \frac{1}{L_f} \int_0^L dz \quad \frac{dW}{dt} \tag{12}$$

where L_f is the length of a specified magnetic field line and z is the coordinate along the field line measured from the midplane. Justification for this averaging procedure is found in Appendix C.

A final parameter is microwave field energy $|E|^2$. Unless otherwise specified, the total electric field strength in Eq. (12) is assumed to be a constant in regions of mode propagation. The relative strength of right-hand, left-hand and parallel electric field polarizations is determined from the cold plasma dispersion relation. In spatial regions where the extraordinary wave

does not propagate the wave amplitude is always set equal to zero. Eq. (12) is also evaluated assuming that the ratio $k_z/k_\perp$, is fixed. The formalism allows both a calculation of relative heating and cooling rates and a calculation of steady state conditions, neglecting spatial diffusion of hot electrons, when:

$$\left\langle \frac{dW}{dt} \right\rangle = \left(P_{sync} + P_{brems} + P_{coll}\right)\Big|_{z = 0} \tag{13}$$

which assumes synchrotron radiation, bremsstrahlung and collisional drag evaluated at the midplane, $z = 0$.

IV. CALCULATION RESULTS

With the aforementioned model for the relativistic bumpy torus annulus, calculations of quasilinear heating and steady state annulus temperatures have been carried out. Results are summarized in Figures 2-10.

Figures 2-5 indicate the spatial regions along the specific magnetic field line where wave particles resonances occur, as a function of ring temperature. A clear feature of the figures is the spatial broadening of the resonance zones and the increasing importance of a greater number of electron-cyclotron harmonics as ring temperatures approach relativistic energies (i.e., $\gtrsim$ 100 keV). Resonance broadening is a consequence of the resonant condition:

$$0 = \omega - n\Omega_o/\gamma - k_z p_z/m\gamma \quad , \tag{14}$$

and the dependence of Eq. (1) on Bessel function values. Three factors cause the broadening. First, in the relativistic regime Eq. (14) is a function of perpendicular and parallel momentum through the relativistic parameter, $\gamma = (1 + p^2/c^2)^{-\frac{1}{2}}$. In particular, electrons which would be nonresonant if Eq. (14) did not depend on γ can become resonant for $\gamma > 1$. Second, the number of particles with parallel velocities approaching the speed of light becomes larger and the factor $k_z p_z/m_o\gamma$ plays a more significant role in the resonance condition, especially if the parallel index of refraction, $k_z c/\omega$, is greater than one. Third, as the argument of the Bessel functions in Eq. (1), $k_\perp p_\perp/m_o\Omega_o$ becomes larger, the Bessel functions become more comparable in magnitude and all polarizations (i.e., E_+, E_-, and E_z) contribute strongly to the quasilinear heating. The impact of additional electron-cyclotron harmonics, besides fundamental and second, on the wave heating of the annulus as annulus temperature is increased is a result of several effects. First, resonance broadening permits Eq. (14) to be satisfied by more particles at the different harmonics. For example, consider the n = 0 (Landau) resonance:

$$1 = (k_z c/\omega)(v_z/c) \quad . \tag{15}$$

Eq. (15) indicates that the parallel index of refraction must be greater than one for the resonance condition to be satisfied. Moreover, it is necessary that v_z/c be nonzero. For the parallel index of refraction approaching one the parameter v_z/c must also approach a value of one. Under such circumstances the resonant electrons are relativistic. Second, as electrons become more energetic the argument of the Bessel functions in Eq. (1) increase in value. Consequently, the Bessel functions which are not of order zero contribute in a finite way to the quasilinear heating. These are precisely the same Bessel functions on which harmonic cyclotron heating with $|n| > 1$ depend so strongly.

The spatial location of wave heating at the various resonances can be associated with the propagation characteristics of the waves. In the second figure for which $T_A = 1$ keV fundamental and second harmonic heating occur near the points where $\omega = \Omega_o$ and $\omega = 2\Omega_o$, respectively. The amplitude of the heating is greater for fundamental as compared to second harmonic heating because of the relatively small electron-cyclotron radius for $T_A = 1$ keV. Also, a consequence of the small Larmor radius is the negligibly small higher harmonic heating. Now the extraordinary wave has the property that wavenumbers on the high magnetic field side of the upper hybrid resonance surface, Eq. (9) with $k_z = 0$, are larger than those on the low field side of the right-hand cutoff surface specified by Eq. (8). (These surfaces are sketched in Figure 1.) Consequently, consistent with Eq. (14), the width of the spatial zone for fundamental heating in Figure 1 is larger than that for second harmonic heating. Also, if the ratio of $k_z^2/(k_\perp^2 + k_z^2)$ used to calculate Figure 1 would be increased, the spatial width of the heating zones would be increased. Conversely, for parallel wavenumber approaching zero the spatial width of the heating zones decreases while their amplitude increases. In the limit of zero parallel wavenumber the heating zones have negligible width about the points where $\omega = \Omega_o$ and $\omega = 2\Omega_o$. The dip in the fundamental heating rate at the point where $\omega = \Omega_o$ is indicated in an approximate way by a dashed line and is a result of the decrease in right-hand wave electric field polarization consistent with the cold plasma dispersion relation using a fixed value for $k_z^2/(k_z^2 + k_\perp^2)$. For perpendicular wavenumber going to zero the width of this dip decreases until there is no dip for $k_\perp = 0$. By comparison, wave tracing calculations show that k_z increases much more rapidly than $k_\perp$ changes as extraordinary waves propagate toward the fundamental cyclotron resonance surface and is rapidly absorbed.[10]

Figure 3 is the same calculation as Figure 2 except that the annulus temperature has been increased to 200 keV. The figure demonstrates the broadening of the fundamental and second harmonic particularly in the throat of each mirror section where the absolute value of the parallel wavenumber is largest. Conversely, appreciable fundamental resonance heating does not occur near the midplane of the mirror sections because

$$1 - \Omega_o/\gamma\omega > (k_z c/\omega)(v_z/c) \tag{16}$$

for most electrons. The reasons for this behavior are related to the wave propagation characteristics and the bumpy torus magnetic field configuration. As noted previously, the parallel index of refraction is less than unity near the midplane, while the parameter v_z/c is always smaller than one. The parameter $\Omega_o/\gamma\omega$ is smaller than unity in the midplane region and decreases in magnitude as the electron energy increases. Moreover, there exists the spatial region with no extraordinary wave energy between the midplane and the nonrelativistic fundamental cyclotron resonance location. Also with regard to the heating at the fundamental electron-cyclotron resonance heating, the dip in the heating rate shown in Figure 2 disappears in Figure 3 because of the contribution to heating by the E_+ and E_z wave fields. Furthermore, significant fundamental heating occurs away from the location where $\omega = \Omega_o$. Consequently, the relative contribution of fundamental heating near the nonrelativistic fundamental resonance location is much less significant for an annulus temperature of 200 keV than for an annulus temperature of 1 keV. Unlike the case of Figure 2, the high annulus temperature permits the heating at harmonic numbers other than for n = 1,2. In particular, the heating zones for n = -1,0, and 3 are plotted in Figure 3. Because heating at the n = -1 and 0 resonances requires that the parallel index of refraction be greater than one, heating with these resonances can only occur on the high field side of the upper hybrid layer.

Figures 4 and 5 are analogous to Figures 2 and 3 except for the fact that the wave polarization considered is ordinary rather than extraordinary. The features of Figures 4 and 5 are analogous to those of Figures 2 and 3 in the sense that the resonances are broadened for higher annulus temperature. In contrast to Figures 1 and 2, the striking feature of Figures 4 and 5 is the dramatic increase in the maximum amplitude of heating by the ordinary wave as the annulus temperature is increased. This effect is a consequence

of the small right-hand electric field polarization characteristic of ordinary waves and the requirement of finite electron-cyclotron radius in order that E_+ and E_z contribute appreciably to heating. Third harmonic heating is not present to an appreciable extent for annulus temperatures of 200 keV because the finite Larmor radius contributions are not large enough that they can compensate for the small right-hand circularly polarized contribution to the ordinary wave heating. No heating by ordinary waves through the n equal zero or negative integer resonances occurs because the parallel index of refraction is always smaller than one for ordinary waves while parallel indices of refraction greater than one are required for heating at these resonances.

Figures 6-10 are plots of the left- and right-hand sides of Eq. (13). Figures 6-9 are for EBT-1 parameters while Figure 10 is appropriate to EBT-S parameters. The intersection of the two curves indicates the ring temperatures at which the quasilinear heating is balanced by losses. For clarity, the various curves in the figures are normalized to the values of $|E|^2$. Hence, the curves representing collisional plus radiation losses move up and down vertically in response to the value of the electric field. Conversely, the curves representing quasilinear heating do not change.

The curves representing the losses reflect the importance of collisional drag and synchrotron radiation. For low annulus temperatures collisional drag is the dominant loss process and the loss rate decreases with annulus temperature at least for nonrelativistic energies. However, for higher relativistic annulus temperatures synchrotron radiation becomes dominant and the loss rate increases with temperature. For all parameters examined bremsstrahlung is negligible compared to collisional drag and synchrotron radiation.

A general feature of Figures 6-10 is that the curves representing the left- and right-hand sides of Eq. (13) intersect at two temperatures. Between the two temperatures quasilinear heating is greater than the ring losses. Hence, if the annulus temperature is below that of the lower intersection point, annulus startup is not possible; however, if the annulus temperature is greater than that at the lower intersection point, the annulus temperature can increase up to the larger intersection point corresponding to the annulus steady-state temperature. Larger annulus temperatures are not possible because ring losses exceed quasilinear heating. Simply stated, the annulus temperature calculated by the model reaches a maximum steady-state value once a threshold temperature

is exceeded. Note also that quasilinear heating by only ordinary waves requires that the annulus temperature exceed a higher threshold value than required by extraordinary waves. Hence, extraordinary waves are much more critical for ring startup than ordinary waves. However, in the relativistic annulus temperature regime both ordinary and extraordinary wave heating are significant.

To illustrate the importance of fundamental heating in determining ring parameters, calculations were made in which wave electric fields were set equal to zero for distances of $z > 6$ cm where z is the coordinate along the field line as measured from the midplane. (The location $z' = 6$ cm is within the cutoff region for extraordinary waves.) Results of these calculations presented in Figure 6 are compared to similar calculations in which finite wave amplitudes for both the ordinary and extraordinary modes are permitted in the throat (see Figure 7). Wall reflection is invoked to account for the extraordinary wave energy in the throat. With the artificial cutoff in wave amplitudes, Figure 6 indicates that ordinary waves alone cannot maintain the annulus for $|E|^2 = 0.2$ erg/cm^3. Extraordinary waves permit an annulus temperature of 230 keV in the figure. In contrast to Figure 6, Figure 7 shows an annulus temperature of approximately 650 and 900 keV for ordinary and extraordinary waves, respectively. Hence, fundamental heating which is a dominant mechanism in the throat has a profound impact on annulus temperature in the model.

Figure 8 assumes ordinary wave energy at all points on the field line while no extraordinary wave energy is permitted on the high field side of the extraordinary wave cutoff specified by Eq. (8). Consequently, unlike Figure 7, mode conversion of ordinary to extraordinary waves by wall reflection is not considered. By comparing Figures 7 and 8 it is evident that without wall reflection the minimum annulus temperature required for startup is an order of magnitude larger than for the case when wall reflection is permitted. This result points to the significance of wall reflection and fundamental electron-cyclotron heating by extraordinary waves in annulus startup. However, the calculation in Appendix B does show that $|E|^2 < 0.1$ ergs/cm^3 for extraordinary waves on the high field side of the fundamental resonance permits annulus startup for $T_A \lesssim 500$ eV and for a wide range of plasma parameters. This apparent difference between Figure 8 and Appendix B is due to the choice of annulus distribution function and to the dip in the heating rate with the

associated reduction of $|E_-|^2$ if $k_z/k_\perp$ is constrained to be a constant value in the evaluation of Eq. (13).

Figures 6 to 10 indicate that for relativistic temperatures the annulus temperature is much more insensitive to field line structure than for lower temperatures. Moreover, the relativistic annulus temperature at larger radial distances is somewhat less than for smaller radii. Relativistic effects are the basis for the form of the curves. In particular, relativistic broadening which is ineffective at low annulus temperatures tends to eliminate spatial effects on annulus temperature. Also, the approximate resonance condition (i.e., $\omega \sim n\Omega_0/\gamma$) implies that magnetic field lines which are closer to the plasma axis require electrons of higher kinetic energy in order that the resonance condition be satisfied. Well below the steady-state annulus temperatures, Figure 9 indicates that the heating rate for field lines at a midpoint radius of 8.4 cm is smaller than at radii of 8.9 or 10.4 cm. This is a reflection of the field line geometry in that there is no intersection with the nonrelativistic second harmonic resonance surfaces at 8.4 cm while at the other radii there is.

To illustrate the significance of background plasma parameters on annulus temperature, we compare Figure 9 (for EBT-1) and Figure 10 (for EBT-S) which are based on the assumption that extraordinary wave propagation only occurs from the midplane to the extraordinary wave cutoff. Ordinary wave propagation and mode conversion by wall reflection are neglected in the figures. The figures indicate that steady-state relativistic ring temperatures are larger for EBT-S than for EBT-1 (i.e., for $|E|^2 = 0.2$ ergs/cm^3, $T_A = 340$ keV for EBT-S and 230 for EBT-1). This scaling is qualitatively but not quantitatively consistent with the experiment (i.e., $T_A \approx 500$ keV for EBT-S and 200 keV for EBT-1) and is a result of the increase in quasilinear heating rate at the relativistic energies for the higher magnetic field EBT-S configuration. In particular, Eq. (8) indicates that extraordinary wave cutoff in EBT-S is located closer to the throat than in EBT-1. Consequently, the size of the cutoff region is reduced in EBT-S relative to EBT-1 and so more extraordinary wave energy is available to heat the annulus in EBT-S.

The power balance relations depicted in Figures 6-10 indicate that, depending upon wave and plasma parameters, approximately 1-2 x 10^5 ergs/cm^3-sec

of microwave power are required to sustain the relativistic annulus. For an annulus volume of 6×10^4 cm^3,[18] the corresponding total power deposition within the annulus lies between 600 - 1200 watts, in agreement with previous estimates.[17,18] It also follows that our assumption of wave electric field strengths corresponding to $|E|^2 \sim .1 - 1$ ergs/cm^3 is on the average reasonable for EBT-1 and EBT-S.

V. CONCLUDING REMARKS

We have presented a model for the relativistic electron annulus in EBT which assumes that the annulus distribution function is an isotropic relativistic Maxwellian. To determine steady-state annulus temperatures, quasi-linear heating of the annulus by microwaves has been balanced with loss terms representing collisional drag synchrotron radiation and bremsstrahlung neglecting spatial diffusion of the hot electron. The results demonstrate that linear second harmonic heating by either extraordinary or ordinary waves does not permit annulus startup for electrons with energies less than 1 keV. However, second harmonic extraordinary wave heating is effective in heating the annulus for $T_A \gtrsim 10^4$ eV, while ordinary wave heating becomes of comparable importance to extraordinary wave heating as electron energy increases. The calculations also indicate that the steady-state annulus temperature depends critically upon the wave electric field strength and the density of the bulk plasma. In particular, they suggest that $|E|^2 \sim .1 - 1$ erg/cm^3 in the second harmonic heating region and smaller values of extraordinary wave energy density in the high field side of the fundamental resonance can account for annulus startup and steady-state. Collisional interaction between the annulus electrons is included only to the extent that the distribution is assumed to remain Maxwellian. Consequently, the calculations do not depend on annulus density.

Neglecting extraordinary wave propagation in the throat beyond the cutoff layer and ordinary wave heating, the calculation gives annulus temperatures on the order of several hundred kilovolts for both EBT-1 and EBT-S, with reasonable values of the wave electric field strength. Moreover, the calculations suggest that the annulus temperature in EBT-S is larger than in EBT-1, consistent with the experimental trends.

To obtain improved quantitative agreement between experiment and calculation, it is necessary that more physics be included in the model. For example, experimental measurements suggest that the perpendicular momentum of annulus electrons is larger than the parallel momentum.[4,25] Moreover, a population of relativistic electrons exist in bumpy tori, displaced from the annulus, with primarily parallel momentum.[4,25] Consistent with the measurements it would be

desirable to permit the annulus electron distribution function to be anisotropic and separate parallel from perpendicular wave heating. Also, boundary layer and loss cone effects as well as better estimates of electric field amplitudes would permit more accurate calculations of annulus parameters. Field line averaging over loss terms as well as quasilinear diffusion would be useful, as well as a knowledge of $\underset{\sim}{E}(r,z)$. At the present time such improvements in the annulus model are being made.

FIGURE CAPTIONS

Figure 1. Sketch of the cutoff and electron-cyclotron resonant regions in EBT-1. This figure is taken from Ref. 10.

Figure 2. Extraordinary wave heating rate for various cyclotron harmonics normalized to $|E|^2$ (units of sec^{-1}) versus distance along field line as measured from midplane (units of cm). The field line chosen is a radial distance of r = 8.9 cm from the axis at the midplane. Crosshatching on abscissa indicates cutoff zone. T_A = 1 keV, $k_z^2/(k_z^2 + k_\perp^2) = 0.5$.

Figure 3. Same as Figure 3 but T_A = 200 keV.

Figure 4. Same as Figure 2 but for ordinary waves.

Figure 5. Same as Figure 3 but for ordinary waves.

Figure 6. Heating rate (dW/dt) normalized to $|E|^2$ and loss rate (dW'/dt) normalized to $|E|^2$ (units of sec^{-1}) versus annulus temperature (units of eV). Extraordinary heating rate, ordinary heating rate and loss rate are indicated by the following types of lines: ———, - - -, and —·—·, respectively. $k_z^2/(k_z^2 + k_\perp^2) = 0.5$, B_o = 4500 gauss, background density = 1.2×10^{12} cm^{-3}, and annulus density = 1×10^{11} cm^{-3}, respectively. Only n = 1 and 2 heating are included. Wave amplitudes are set equal to zero for z' > 6 cm. All curves are evaluated for the magnetic field line located at r = 8.9 cm from axis at the midplane.

Figure 7. Same as Figure 6 but wave field amplitudes in the throat are permitted to be finite.

Figure 8. Same as Figures 6 and 7 for the extraordinary and ordinary waves, respectively. Two values of the wave electric field strength are assumed for each polarization: $|E|^2$ = .2 and 1 erg/cm^3. The average heating rate between extraordinary and ordinary wave heating is represented by ····· .

Figure 9. Same as Figure 6 for the extraordinary wave heating rate which is evaluated for three midplane radii of field lines r = 8.4, 8.9 and 10.4 cm. Loss expression is evaluated for r = 8.9 cm. $|E|^2$ = 0.2 and 1 erg/cm^3.

Figure 10. Same as Figure 9 but for EBT-S parameters: B_o = 7000 gauss and $\omega/2\pi$ = 28 GHz. Heating rates are evaluated for magnetic field lines located at two midplane radii: r = 8.9 and 10.4 cm. $|E|^2$ = 0.1, 0.2 and 1 erg/cm^3.

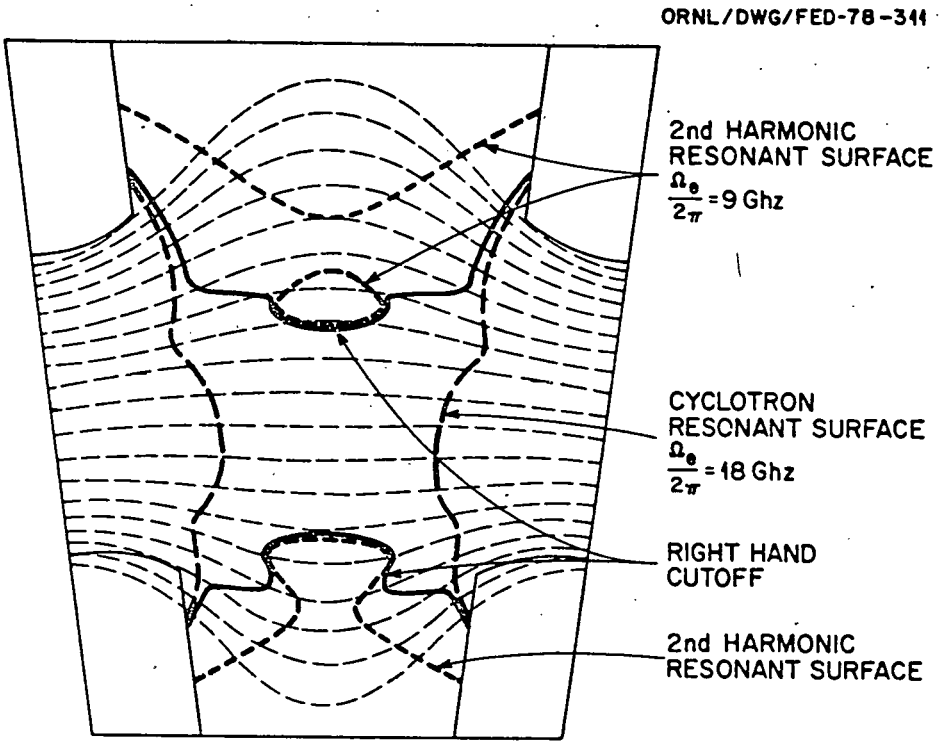
ORNL/DWG/FED-78-341
2nd HARMONIC
RESONANT SURFACE
$\frac{\Omega_e}{2\pi}$ = 9 Ghz
CYCLOTRON
RESONANT SURFACE
$\frac{\Omega_e}{2\pi}$ = 18 Ghz
RIGHT HAND
CUTOFF
2nd HARMONIC
RESONANT SURFACE

Figure 1

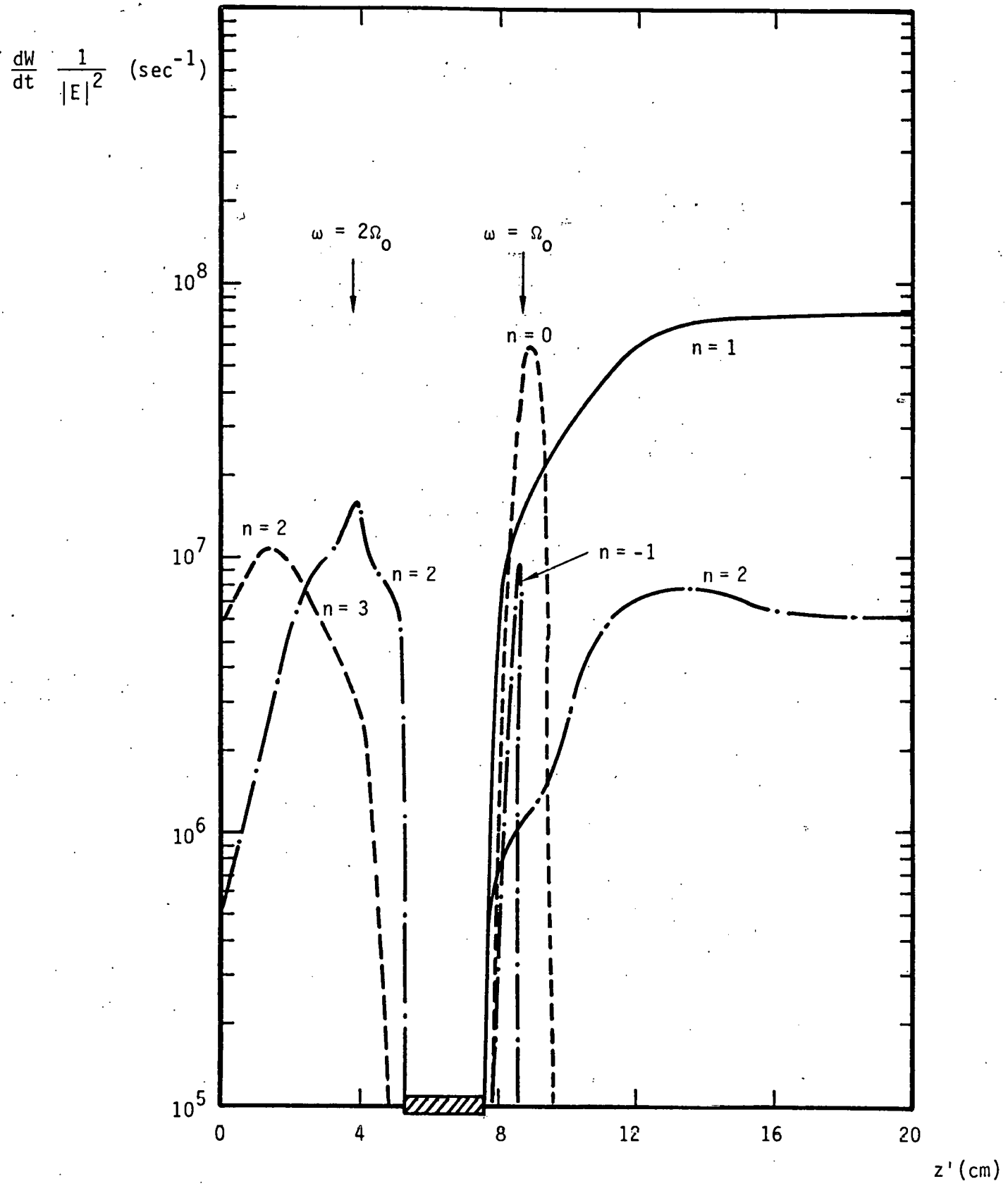
$\frac{dW}{dt}\ \frac{1}{|E|^2}$ (sec^{-1})
$\omega = 2\Omega_o$
$\omega = \Omega_o$
10^8
10^7
10^6
10^5
n = 0
n = 1
n = 2
n = 3
n = 2
n = -1
n = 2
0
4
8
12
16
20
z'(cm)

Figure 2

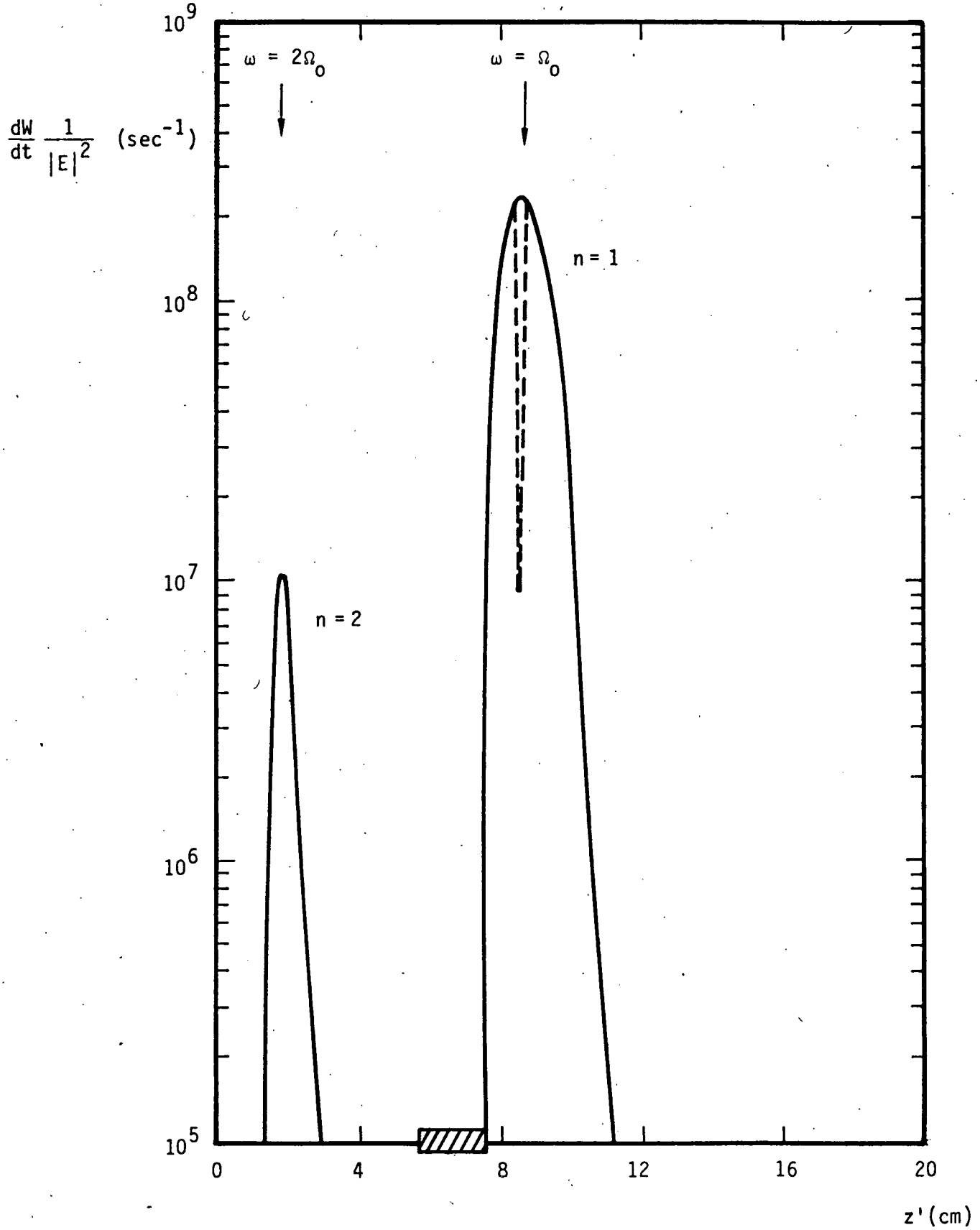
10^9
10^8
10^7
10^6
10^5
$\frac{dW}{dt}\frac{1}{|E|^2}$ (sec^{-1})
$\omega = 2\Omega_o$
$\omega = \Omega_o$
n = 1
n = 2
0
4
8
12
16
20
z'(cm)

Figure 3

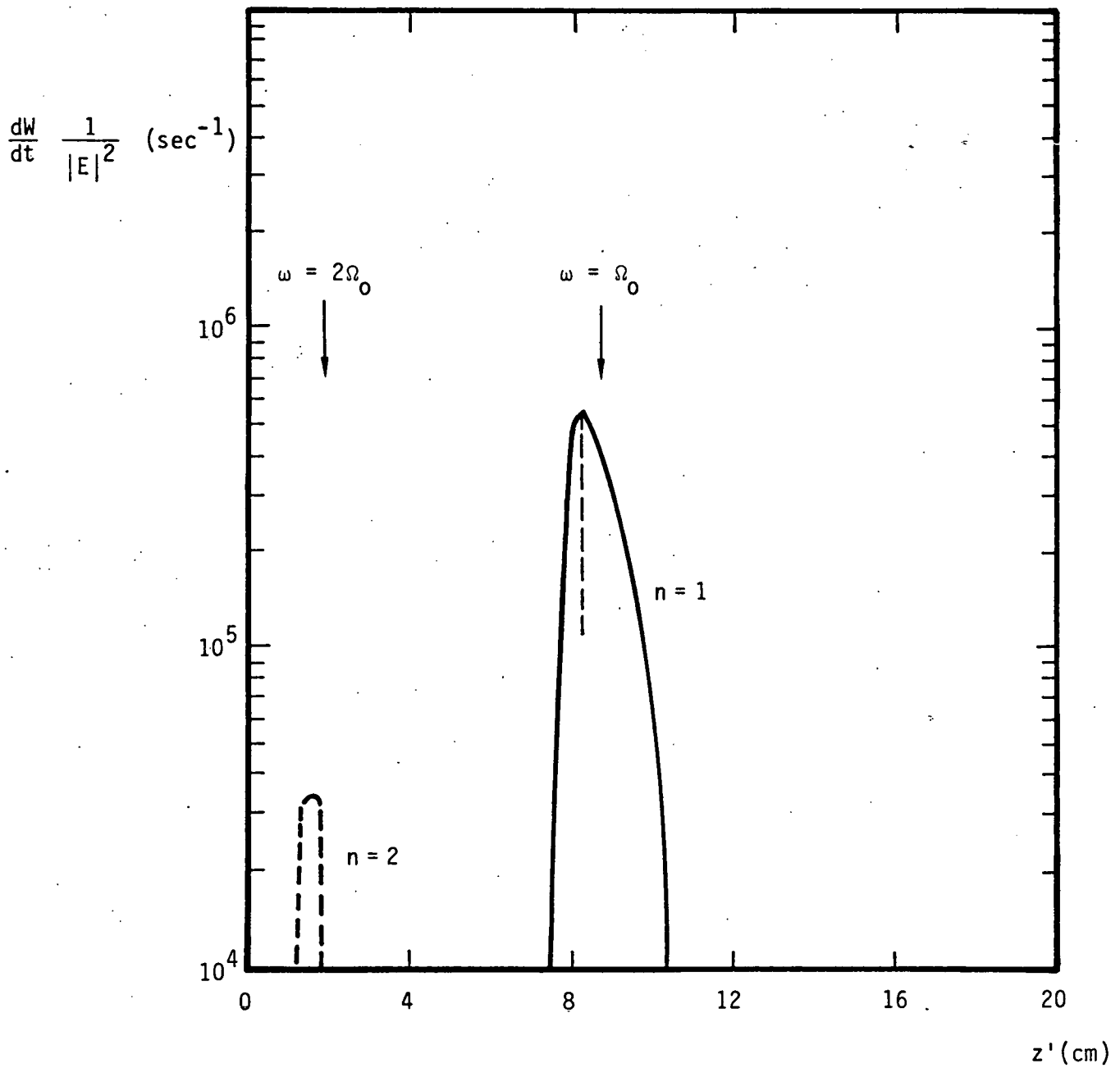
$\frac{dW}{dt}\ \frac{1}{|E|^2}\ (sec^{-1})$
$\omega = 2\Omega_o$
$\omega = \Omega_o$
10^6
10^5
10^4
n = 1
n = 2
0
4
8
12
16
20
z'(cm)

Figure 4

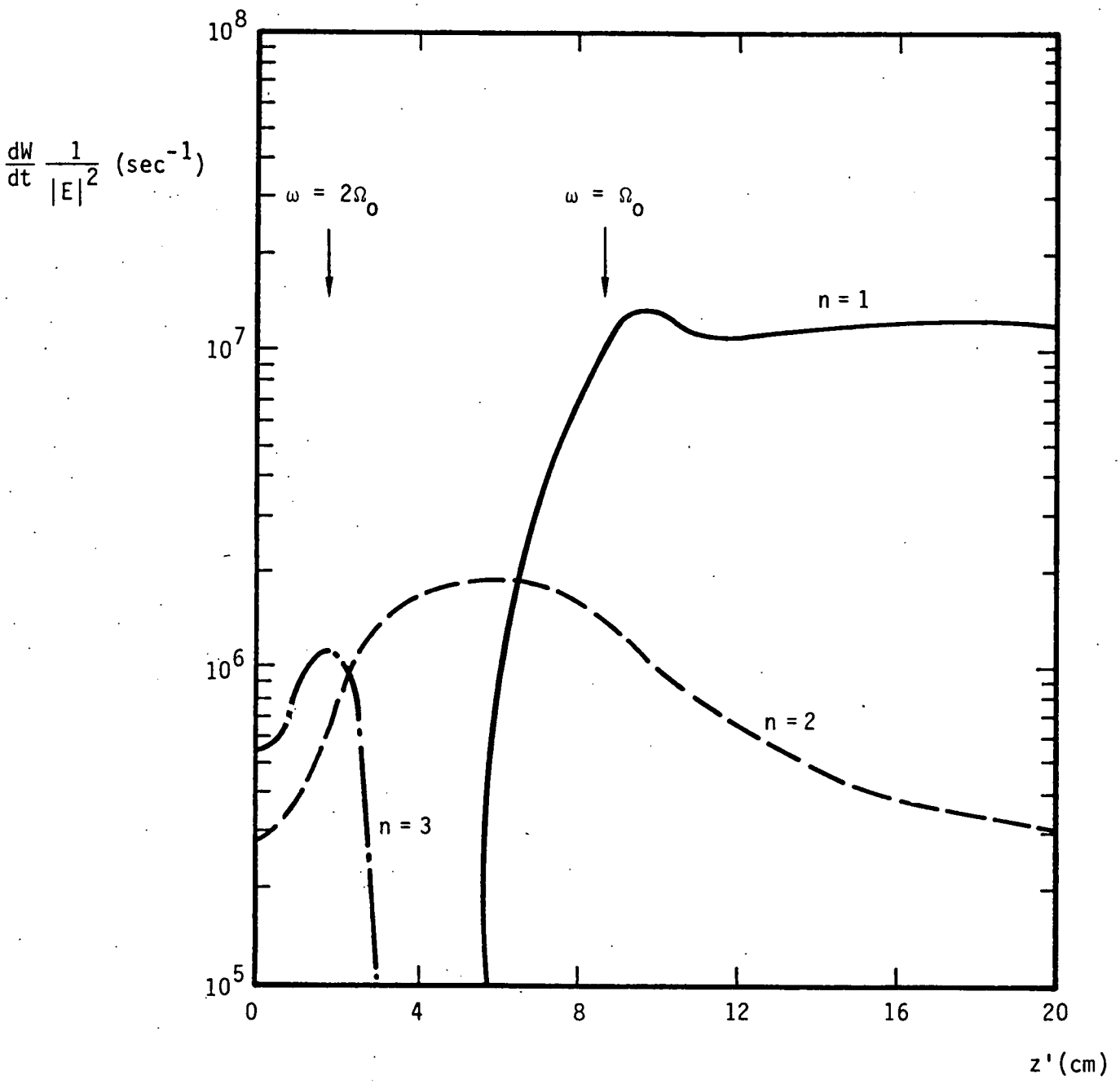
$\frac{dW}{dt}\frac{1}{|E|^2}$ (sec^{-1})
10^8
10^7
10^6
10^5
$\omega = 2\Omega_o$
$\omega = \Omega_o$
n = 1
n = 2
n = 3
0
4
8
12
16
20
z'(cm)

Figure 5

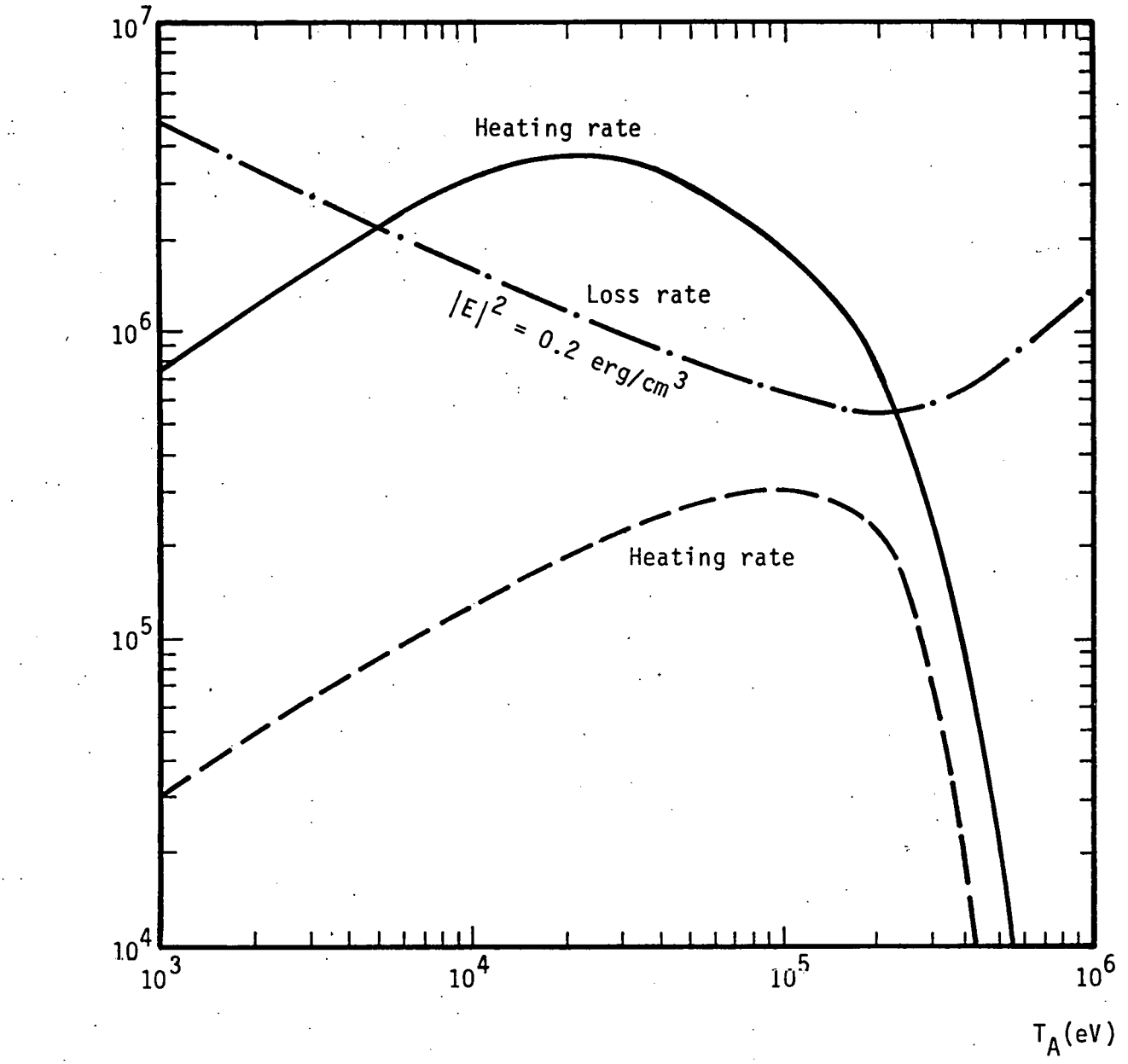
$\frac{dW}{dt}\frac{1}{|E|^2}$, $\frac{dW'}{dt}\frac{1}{|E|^2}$ (sec^{-1})
10^7
10^6
10^5
10^4
Heating rate
Loss rate
$|E|^2 = 0.2$ erg/cm^3
Heating rate
10^3
10^4
10^5
10^6
T_A(eV)

Figure 6

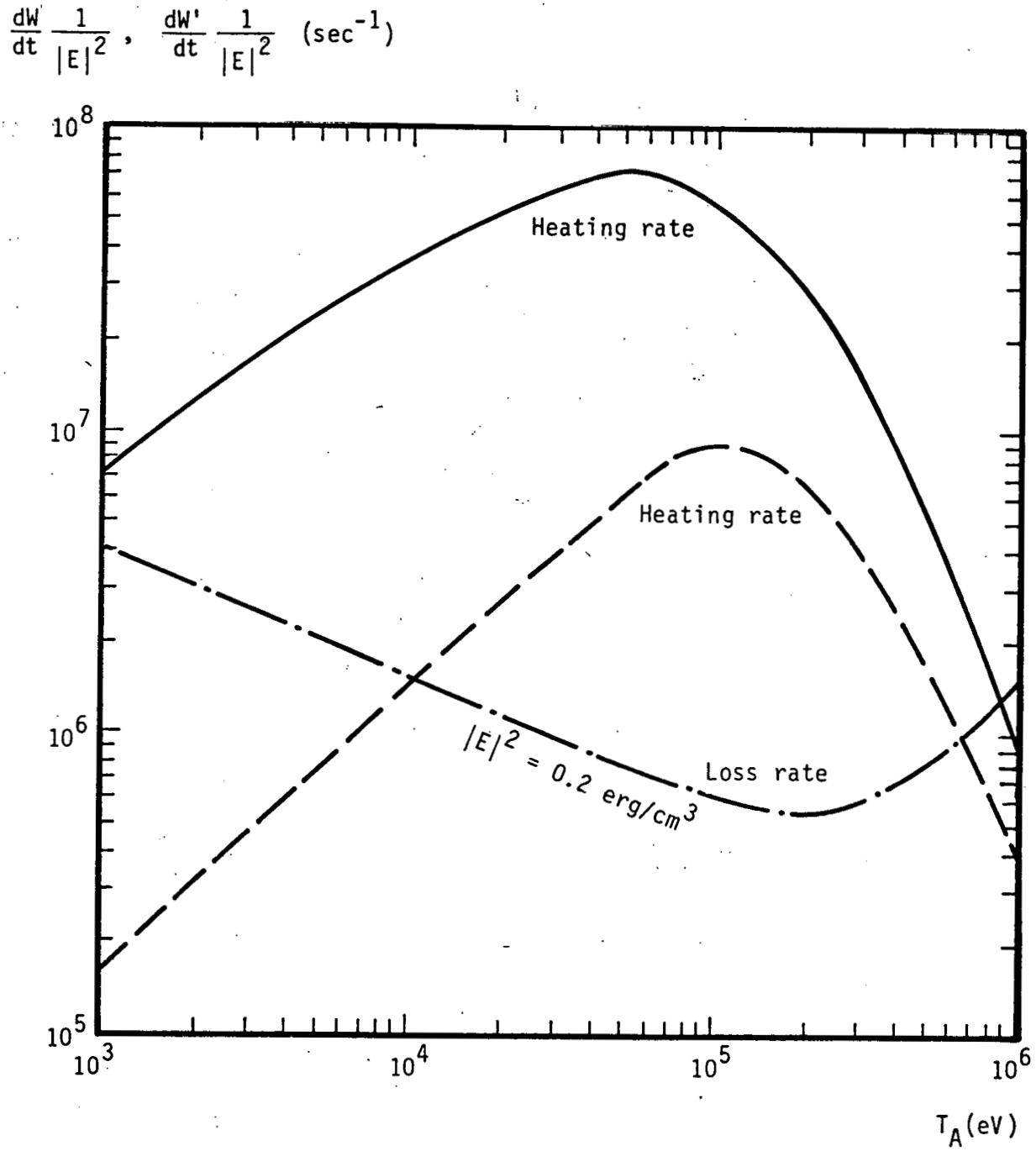
$\frac{dW}{dt}\frac{1}{|E|^2}$, $\frac{dW'}{dt}\frac{1}{|E|^2}$ (sec^{-1})
10^8
10^7
10^6
10^5
10^3
10^4
10^5
10^6
Heating rate
Heating rate
Loss rate
$|E|^2 = 0.2$ erg/cm^3
T_A(eV)

Figure 7

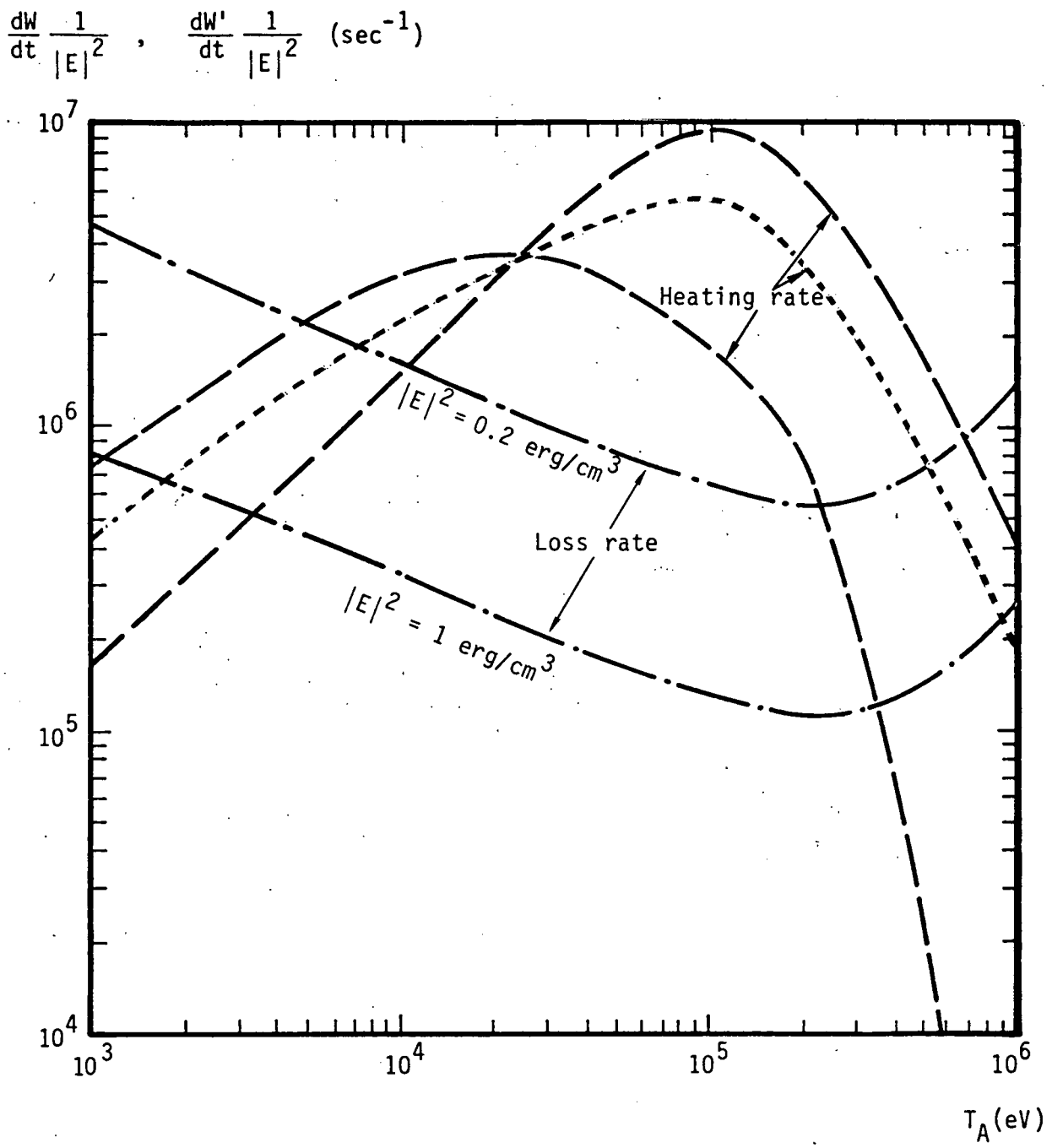
$\frac{dW}{dt}\frac{1}{|E|^2}$, $\frac{dW'}{dt}\frac{1}{|E|^2}$ (sec^{-1})
10^7
10^6
10^5
10^4
10^3
10^4
10^5
10^6
$T_A(eV)$
Heating rate
$|E|^2 = 0.2$ erg/cm^3
Loss rate
$|E|^2 = 1$ erg/cm^3

Figure 8

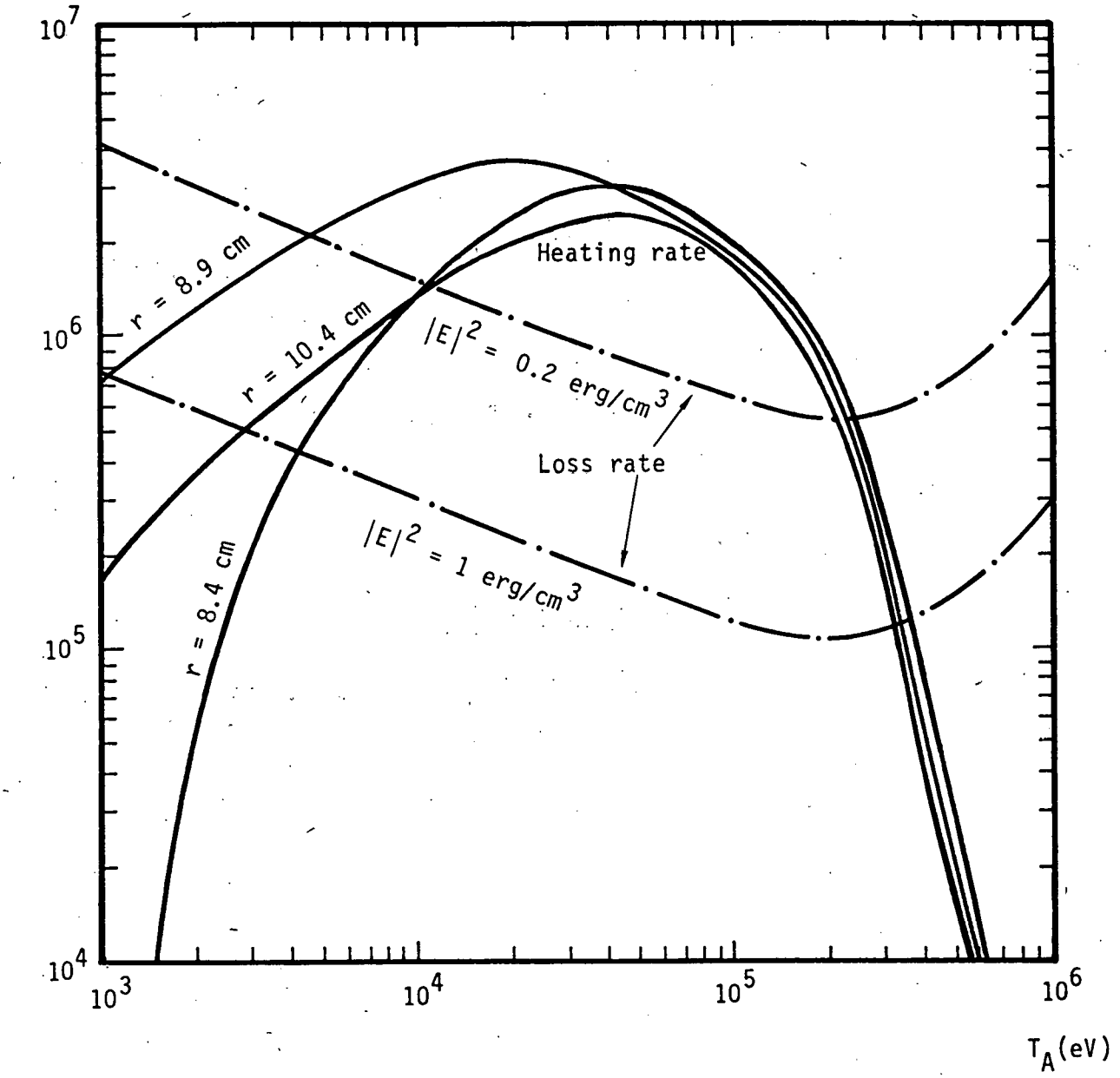
$\frac{dW}{dt}\frac{1}{|E|^2}$, $\frac{dW'}{dt}\frac{1}{|E|^2}$ (sec^{-1})
10^7
10^6
10^5
10^4
10^3
10^4
10^5
10^6
T_A(eV)
r = 8.9 cm
r = 10.4 cm
r = 8.4 cm
Heating rate
$|E|^2$ = 0.2 erg/cm^3
Loss rate
$|E|^2$ = 1 erg/cm^3

Figure 9

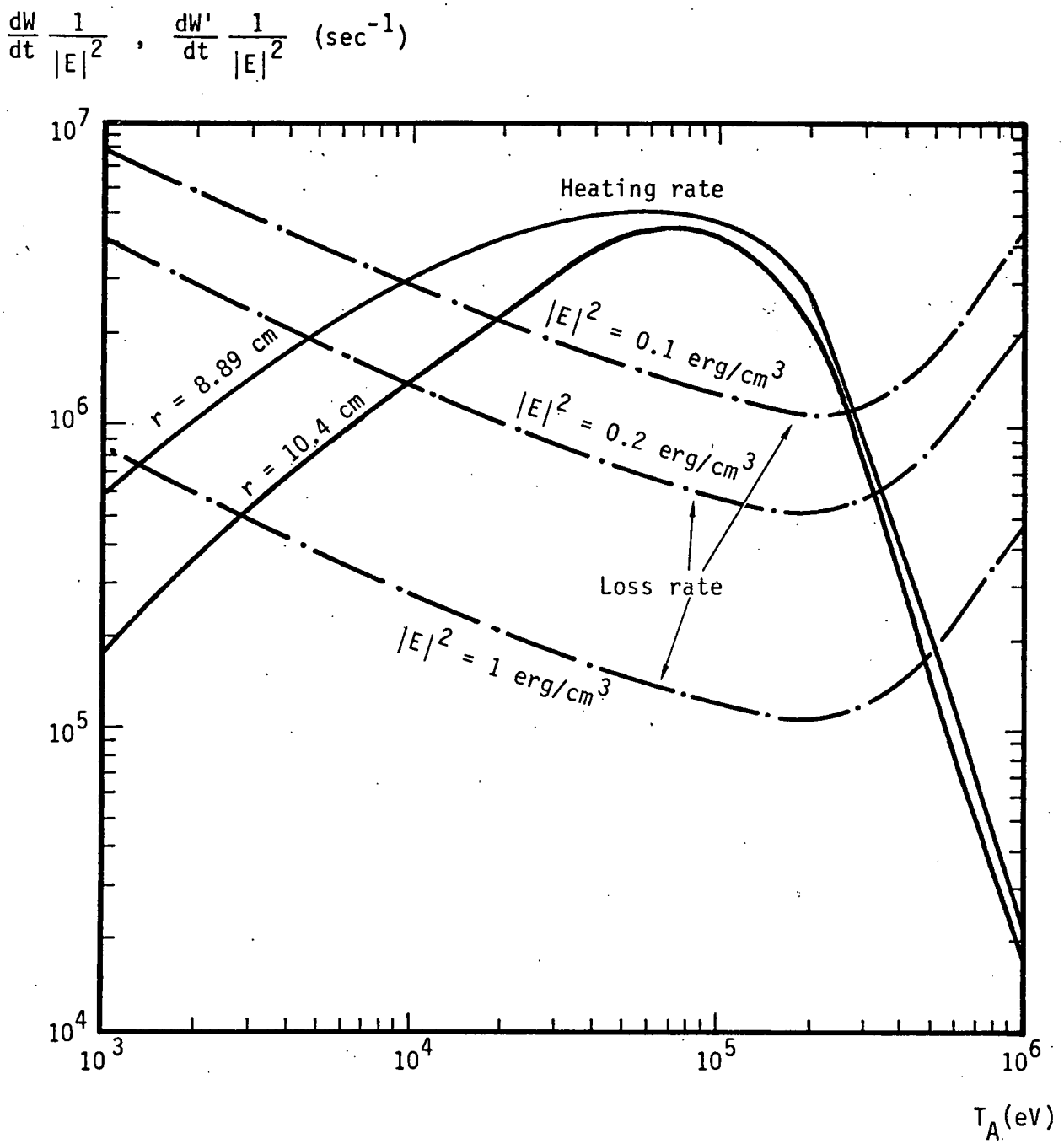
$\frac{dW}{dt}\frac{1}{|E|^2}$, $\frac{dW'}{dt}\frac{1}{|E|^2}$ (sec^{-1})
10^7
10^6
10^5
10^4
10^3
10^4
10^5
10^6
$T_A(eV)$
Heating rate
r = 8.89 cm
r = 10.4 cm
$|E|^2$ = 0.1 erg/cm^3
$|E|^2$ = 0.2 erg/cm^3
$|E|^2$ = 1 erg/cm^3
Loss rate

Figure 10

APPENDIX A. MODE CONVERSION BY WALL REFLECTION

To generate electrons of sufficiently high energy which can be effectively heated at the second and higher electron-cyclotron harmonics, it is necessary to overcome the strong collisional drag on cold electrons. The damping of extraordinary waves at the fundamental can have this effect. However, because extraordinary waves cannot propagate directly to the fundamental resonance zones from launching structures at the midplane it is necessary to invoke a mode conversion process from ordinary to extraordinary polarization. One powerful mode conversion mechanism is the reflection of ordinary modes off the conducting walls. In this appendix it is shown that for almost all angles of propagation substantial mode conversion occurs.

Consider the plane geometry of Figure A-1. A plane incident wave with wavenumber $\vec{k}_o$ and originating at $x > 0$ impinges upon a reflecting wall at $x = 0$. This wave is then reflected into two waves with wavenumbers $\vec{k}_1$ and $\vec{k}_2$, respectively. The background magnetic field is assumed to be z-directed. All wavenumbers are presumed to lie in the x-z plane and to correspond to wave propagation.

Because two modes of propagation exist in the cold magnetized plasma approximation it follows that:

$$|\vec{k}_o| = |\vec{k}_1| \neq |\vec{k}_2| \quad . \tag{A-1}$$

Furthermore, Snell's law requires that

$$k_{oz} = k_{1z} = k_{2z} \tag{A-2}$$

where subscript z denotes magnetic field aligned component. Considering only forward propagating solutions to the dispersion relation it follows that:

$$k_{1x} = -k_{ox} \quad ,$$

$$k_{1x}\, k_{ox} < 0 \tag{A-3}$$

where subscript x denotes the component parallel to the normal of the reflecting plane. For the x-, y- and z-directed electric field components of the three waves [i.e., (E_{ox}, E_{oy}, E_{oz}), (E_{1x}, E_{1y}, E_{1z}) and (E_{2x}, E_{2y}, E_{2z})], Maxwell's equation implies the following relation:

$$0 = E_{oy} + E_{1y} + E_{2y} \tag{A-4a}$$

$$0 = E_{oz} + E_{1z} + E_{2z} \quad . \tag{A-4b}$$

These expressions can be related to each other through the cold plasma dispersion relation:[24]

$$0 = (S - n_x^2)\, E_x - iD\, E_y + n_x\, n_z\, E_z \tag{A-5a}$$

$$0 = iD\, E_x + (S - n_x^2 - n_z^2)\, E_y \tag{A-5b}$$

$$0 = n_x\, n_z\, E_x + (P - n_x^2)\, E_z \tag{A-5c}$$

with

$$S = 1 - \frac{\omega_{pe}^2}{\omega^2 - \Omega_o^2} \quad , \quad D = - \frac{\Omega_o\, \omega_{pe}^2}{\omega\, (\omega^2 - \Omega_o^2)} \quad ,$$

$$P = 1 - \frac{\omega_{pe}^2}{\omega^2} \quad , \quad n_x = k_z\, c/\omega \quad , \quad n_z = k_z\, c/\omega \quad . \tag{A-6}$$

Hence,

$$0 = \alpha_o\, (E_{ox} + E_{1x}) + \alpha_2\, E_{2x} \tag{A-7a}$$

$$0 = \beta_o\, (E_{ox} - E_{1x}) - \beta_2\, E_{2x} \tag{A-7b}$$

with

$$\alpha_o = D/(S - n_{ox}^2 - n_{oz}^2) \quad , \quad \alpha_2 = D/(S - n_{2x}^2 - n_{2z}^2) \quad ,$$

$$\beta_o = n_{ox}\, n_{oz}/(P - n_{ox}^2) \quad , \quad \beta_2 = |n_{2x}|\, n_{oz}/(P - n_{2x}^2) \quad . \tag{A-8}$$

In terms of E_{ox},

$$E_{1x} = [(\beta_o/\beta_2) - (\alpha_o/\alpha_2)][(\beta_o/\beta_2) + (\alpha_o/\alpha_2)]^{-1} E_{ox} \qquad \text{(A-9a)}$$

$$E_{2x} = 0.5\ [(\beta_2/\beta_o) - (\alpha_2/\alpha_o)]\ E_{ox} \quad . \qquad \text{(A-9b)}$$

The efficiency of conversion can now be defined in the following way:

$$E \equiv 1 - |E_{1x}|^2/|E_{ox}|^2 \quad . \qquad \text{(A-10)}$$

This efficiency is plotted in Figures A-2 and A-3 for conversion of extraordinary to ordinary polarizations and ordinary to extraordinary polarizations, respectively, conversion efficiencies in excess of ten percent for all angles of propagation except those approaching zero or ninety degrees. The reason for the lack of mode conversion at ninety degree propagation is the pure magnetic field aligned polarization of ordinary waves while the extraordinary waves have wave electric fields only perpendicular to the ambient magnetic field. Similarly at zero degrees both waves have no z-directed electric field and so no mode conversion occurs (i.e., Eq. (A-7b) is trivial). In any case for EBT, wave propagation will generally be oblique to the magnetic field for wave launching in midplane and so substantial mode conversion should occur.

An interesting feature of Figure A-2 is that the $\cos^2(\theta) \to 1$ mode conversion of extraordinary waves leads to surface ordinary waves. Hence, the curves are not extended to these large values of $\cos^2(\theta)$. Surface wave generation through reflection off conducting walls will be discussed in a future publication.

FIGURE CAPTIONS

Figure A-1. Model for calculations in Appendix A.

Figure A-2. Plot of efficiency for mode conversion of extraordinary to ordinary waves versus $\cos^2(\theta) = k_z^2/k_\perp^2 + k_z^2)$. Background density is 4×10^{11} cm^{-3}; $\omega = 2\pi \times 18$ GHz; $\omega_{pe}^2/\omega^2 = 0.1$; $\Omega_o/\omega = 1.1$ (———), 1.4 (- - -) and 2.0 (—•—•).

Figure A-3. Same as Figure A-2 but for conversion of ordinary to extraordinary waves.

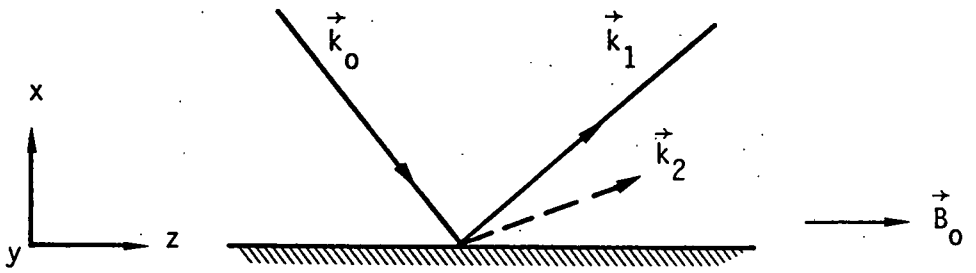

Figure A-1

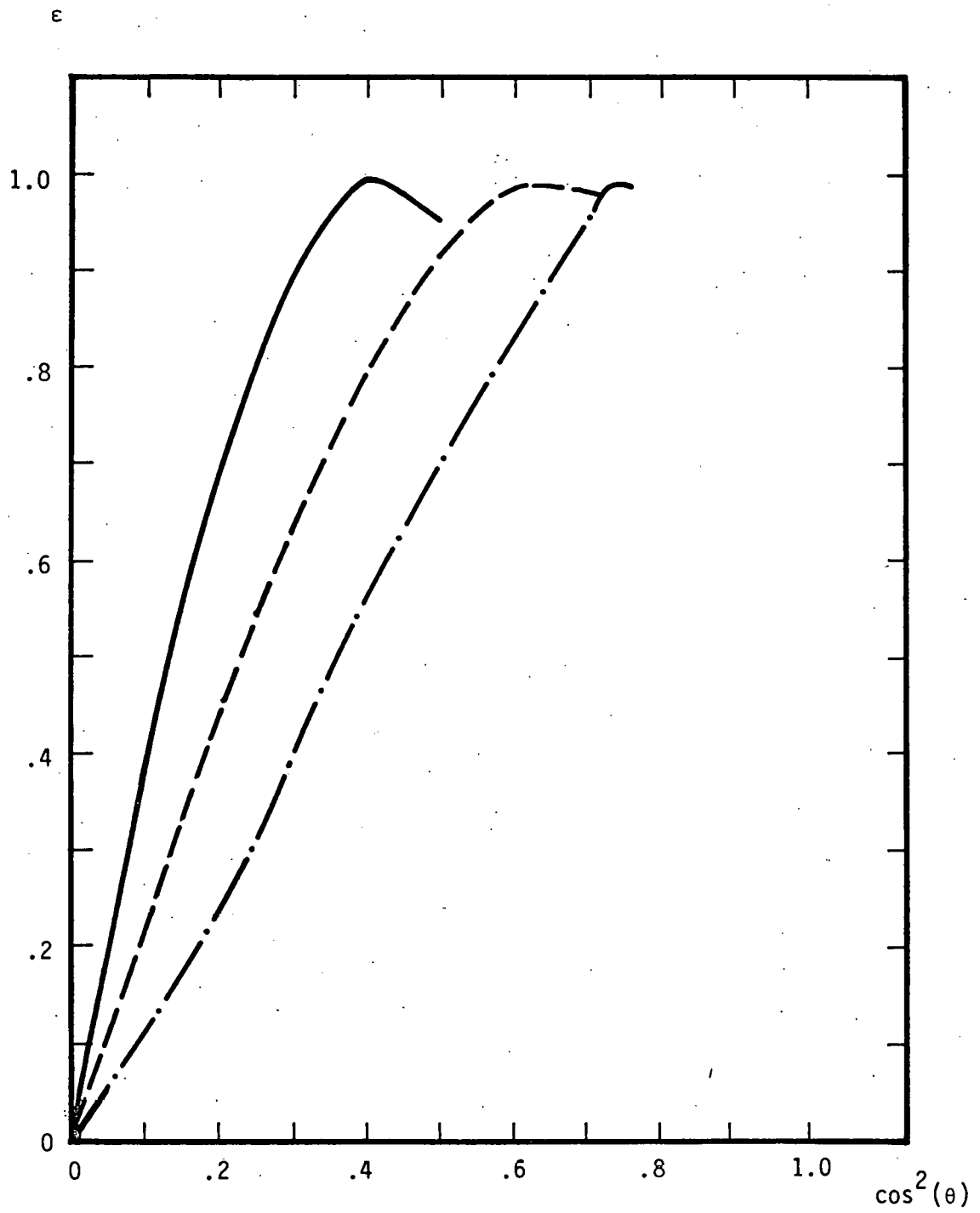

Figure A-2

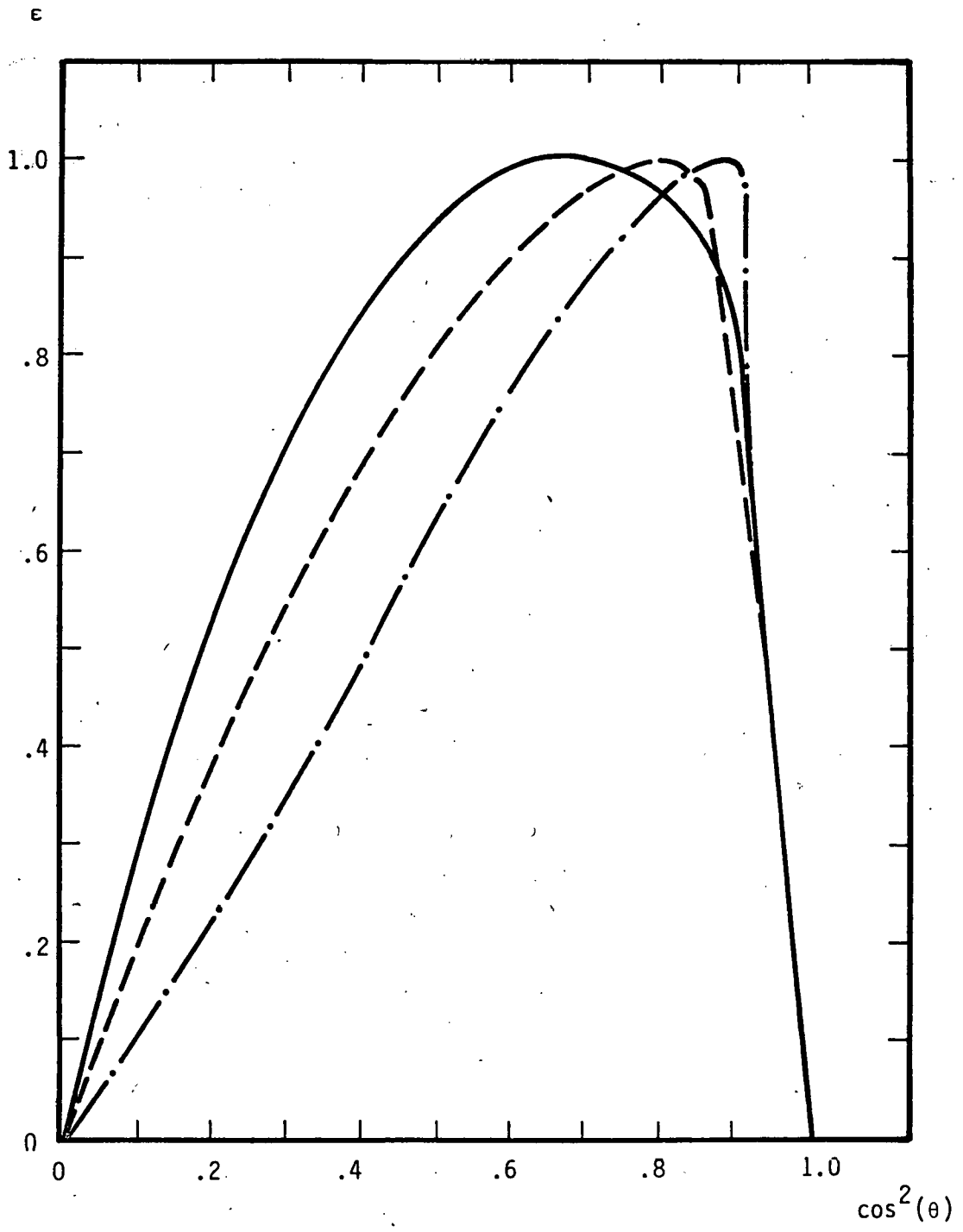

Figure A-3

APPENDIX B. ANNULUS STARTUP THROUGH FUNDAMENTAL HEATING

In order that electrons can be heated by second and higher harmonic electron-cyclotron damping to the relativistic energies appropriate to the electron annulus, a mechanism must be available to increase the perpendicular energy of electrons. Fundamental electron-cyclotron damping is such a mechanism. Several features of the fundamental heating process make it especially attractive. First, it is a linear process which takes place even for finite wave amplitudes. Second, fundamental heating occurs even for the very cold electrons nearly zero electron gyro-radius. This feature is in contrast to second and higher harmonic heating which requires electrons to have finite electron gyro-radii. Third, for a magnetically confined plasma geometry fundamental heating only requires that the wave frequency equal the nonrelativistic electron-cyclotron frequency at discrete locations along a magnetic field line.

In this appendix it is shown that fundamental electron-cyclotron heating of electrons in the tail of the electron distribution function for cold electrons is sufficient to overcome collisional drag and to accelerate electrons in the perpendicular direction. Consequently, these electrons can reach perpendicular velocities sufficient for higher harmonic heating to become appreciable.

For electrons in the tail of the electron distribution function, the fundamental electron-cyclotron interaction occurs when:

$$\omega - \Omega_o = k_{\parallel} v_{\parallel} \tag{B-1}$$

where $v_{\parallel}$ is the parallel electron velocity. Because Eq. (B-1) is satisfied for a specific electron at a discrete location along a field line, it can be anticipated that the wave amplitude is sensibly constant as far as wave energy absorption by the single electron is concerned. Hence, a weak wave absorption model is appropriate for a single electron with the field line averaged rate of wave energy absorption by a single electron given by:[26,27]

$$P_1 = 2\pi N \frac{L_1}{L_f} \frac{ec}{B_o} |E_-|^2 \qquad \text{(B-2)}$$

where L_1 is the field aligned gradient of the magnetic field strength. This expression corresponds to two resonance zones per mirror section and N mirror sections.

The rate at which tail electrons lose energy due to collisions with background electrons is given by:[28]

$$P_2 = \frac{4\pi n e^4}{mv} \ln (\Lambda) \qquad \text{(B-3)}$$

where the background electron temperature, background electron density, and tail electron speed are represented by T_e, n and v, respectively. Also,

$$\Lambda = \left(\frac{T_e}{8\pi n}\right)^{\frac{1}{2}} \frac{mv^2}{2e^3} \quad . \qquad \text{(B-4)}$$

For tail electrons to overcome the effects of collisional drag as a result of fundamental electron-cyclotron heating, it is necessary that:

$$P_2 < P_1 \qquad \text{(B-5)}$$

or

$$\frac{2 n e^3 B_o}{m c v} \ln (\Lambda) < \frac{NL_1}{L_f} |E_-|^2 \quad . \qquad \text{(B-6)}$$

Noting that,

$$|k_{\parallel} v_{\parallel}| << \omega \approx \Omega_o \qquad \text{(B-7)}$$

permits Eq. (B-6) to be rewritten as

$$\frac{L_f}{NL_1} \frac{(2m)^{\frac{1}{2}} n \omega e^2}{|E_-|^2} \ln (\Lambda) < w^{\frac{1}{2}} \qquad \text{(B-8)}$$

where the parameter, w, is the tail electron kinetic energy which is assumed to be much larger than T_e. It follows that the capability to overcome drag is

benefited by high electron kinetic energy, low frequency, low background density, large ratio of magnetic field line gradient scale length to magnetic field line length and large values of the right-hand circularly polarized component of the wave electric field. Specifically, for $\omega = 2\pi \times 18$ GHz, and $T_e = 50$ eV, the criterion for tail electron runaway is plotted in Figure B-1. Justification for the arbitrary choice of value for electron temperature is the requirement that $\ln(\Lambda)$ be given some value and the weak dependence of logarithm on plasma parameters.

The values of electric field specified by Figure B-1 can be compared to an estimate of the extraordinary wave electric field expected within the mirror throat. Consider wave propagation exactly parallel to the magnetic field. Based on ray tracing results such propagation is especially appropriate as waves approach the resonant surfaces.[10] The dispersion relation of extraordinary waves is then given by:[10,24]

$$\frac{k_{\parallel}c}{\omega}^2 = 1 + \frac{\omega_{pe}^2}{\omega(\Omega_o - \omega)} \qquad \text{(B-9)}$$

where ω_{pe} is the electron plasma frequency. The Poynting flux for the waves along the magnetic field is:

$$S = \frac{c}{4\pi}\left(\frac{k_{\parallel}c}{\omega}\right)|E_-|^2 \qquad \text{(B-10)}$$

and so the total flux of energy incident on a resonant surface where wave absorption occurs is:

$$S_T = SA = \frac{c}{4\pi} A \left(\frac{k_{\parallel}c}{\omega}\right)|E_-|^2 \qquad \text{(B-11)}$$

where A is the area of the resonant surface. Consider a typical estimated value for the bulk heating rate, 16 kW,[4] then because there are N = 24 mirror sections, two bulk resonant surfaces per section, Eq. (B-11), and surface area A of approximately 350 cm^2, the electric field strength satisfying Eq. (B-11) is:

$$4 \times 10^{-3} \text{ erg/cm}^3 \approx |E_-|^2 (k_{\parallel}c/\omega) \qquad \text{(B-12)}$$

Since Eq. (B-9) implies that $k_{\parallel}c/\omega$ is greater than one it follows that Eq. (B-12) can be rewritten as:

$$|E_-|^2 \lesssim 4 \times 10^{-3} \text{ erg/cm}^3 \quad . \tag{B-13}$$

It follows from the values of electric field (under the assumption of $NL_1/L_f \approx 1$) specified by Figure B-1 that runaway of tail electrons through fundamental electron-cyclotron heating are consistent with the value derived from the experimental measurements, Eq. (B-13). This result is especially true for low background electron density and high tail electron energy. Under such conditions collisional drag is weakest. Also, the dependence of the parallel index of refraction on plasma parameters declines as density decreases. In the limit of zero density the parallel index of refraction approaches one and the wave electric fields attain the maximum value given in Eq. (B-13).

FIGURE CAPTIONS

Figure B-1. Plot of curves indicating boundary for values of ω (eV) and $NL_1/L_f\ |E_-|^2$ (erg/cm^3) which permit Eq. (B-8) to be satisfied for different background densities (i.e., n = 10^{10} cm^{-3} ———, 10^{11} cm^{-3} - - -, and 10^{12} cm^{-3} —·—·). Specifically, values of ω and $NL_1/L_f\ |E_-|^2$ to the right of each of the appropriate curves fulfill the criterion given by the equation.

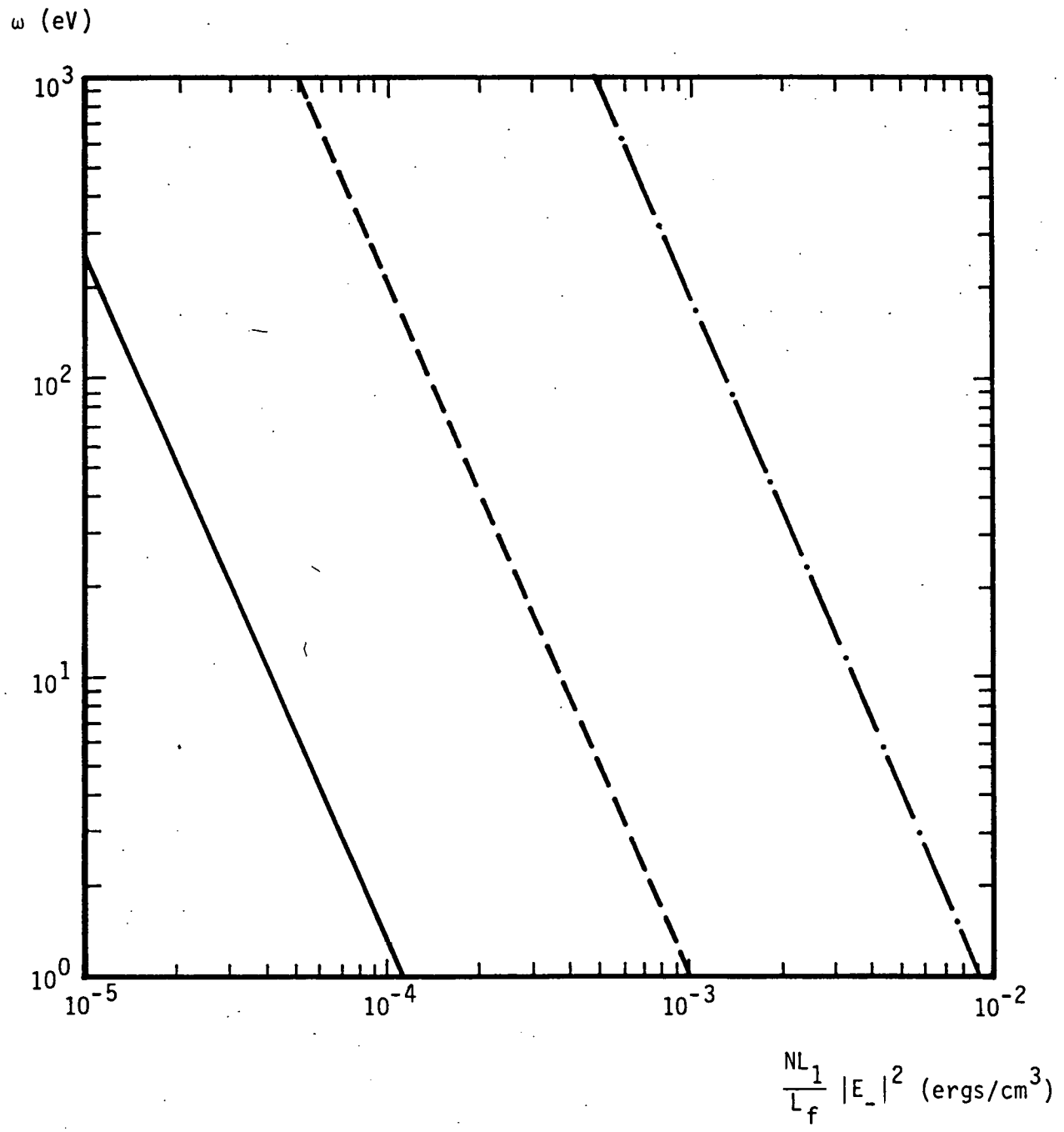

Figure B-1

APPENDIX C. JUSTIFICATION OF QUASILINEAR APPROACH IN MICROWAVE ELECTRON RING HEATING

The use of the uniform-B quasilinear approach has previously[19] been justified for the calculation of ion heating in the inhomogeneous B-field of a tokamak. In that proof, ion particles were assumed to be traveling across magnetic fields.

Similarly we can show that the uniform-B quasilinear calculation can be used for microwave electron ring heating in EBT. In this calculation we assume that electrons are gyrating around, traveling along the nonuniform magnetic field line.

The equation of motion for a single nonrelativistic electron is:

$$\frac{dv_x}{dt} - \Omega(z)\, v_y = \frac{e}{m} E_x \cos(\omega_o t - k_z z) \tag{C-1}$$

$$\frac{dv_y}{dt} + \Omega(z)\, v_x = \frac{e}{m} E_y \sin(\omega_o t - k_z z) \tag{C-2}$$

where $\hat{z}$ direction is set along $\underset{\sim}{B}(z)$; $\Omega(z) = eB(z)/mc$; and ω_o is the applied microwave frequency. With introduction of new variables $E^{\pm} = 1/(2)^{\frac{1}{2}}(E_x \pm E_y)$, $U^{\pm} = v_x \pm i\, v_y$, we have the equation of motion for the right-hand wave as:

$$\frac{dU^-}{dt} - i\,\Omega U^- = \frac{e}{m} E^- e^{i(\omega_o t - k_z z)} \quad . \tag{C-3}$$

We assume that at $t = t_o$ the particle is at $z = z_o$ traveling along z with velocity U_o.

$$z = z_o + (t = t_o)\, U_o$$

$$\Omega(z) = \Omega(z_o) + \frac{d\Omega}{dz}(t = t_o)\, U_o \quad .$$

We may assume that at $t = t_o$ the particle is exactly at the resonant with the applied microwave frequency, $\Omega(z_o) \equiv \omega = \omega_o + k_z U_o$. Then the solution to the equation of motion (C-3) becomes:

$$U^-(t) = U(-\infty) + \frac{e}{m} E^- \; e^{i\int_{t_o}^{t} \Omega \, dt - i k_z z} \int_{-\infty}^{t} dt'$$

$$\exp\left[\frac{i \frac{d\Omega}{dz} (t' - t_o)^2}{2}\right]$$

$$U(-\infty) + \frac{e}{m} E^- \; e^{i\omega t} \left[\frac{2\pi i}{d\Omega/dz}\right]^{\frac{1}{2}} \quad .$$

The energy gain is:

$$E = \frac{m}{2} \langle U(t) \; U^*(t) \rangle - \frac{m}{2} \langle U(-\infty) \; U^*(-\infty) \rangle$$

$$= \frac{m}{2} \langle U(t) \; U^*(t) \rangle \approx \frac{m}{2} \; \frac{e^2}{m^2} \; |E^-|^2 \; \frac{2\pi}{\frac{d\Omega}{dz} U_o} \quad .$$

We have assumed random phase for $U(-\infty)$, so that $\langle U(-\infty) \; E^- \; e^{i\omega t} \rangle \approx 0$.

The number of particles which pass through $z = z_o$ with velocity between U_o and $U_o + dU$ per area dx dy per unit time is $\delta N = dU \; U_o \iint f(x,y,z,v_x,U_o)$ $dv_x \; dv_y$ (dx dy). Knowing resonant condition $U_o = \frac{\omega - \omega_o}{k_z}$, we may express:

$$U_o + dU = \frac{\Omega(z) - \omega_o}{k_z} = \frac{d\Omega}{dz} \; \frac{dz}{k_z} + U_o \quad .$$

Thus

$$dU = \frac{d\Omega}{dz} \; \frac{dz}{k_z} \quad .$$

Substituting

$$\delta N = \int dv_x \int dv_y \; f(x,y,v_x,v_y,U_o) \; \frac{1}{k_z} \; \frac{d\Omega}{dz} \; dx \; dy \; dz \quad .$$

The total energy gain per unit time per volume (dx dy dz) is:

$$P \; dx \; dy \; dz = \delta E \; \delta N \quad .$$

Therefore the total energy gain per unit time per unit volume becomes:

$$P = \frac{\pi e^2}{m} |E^-|^2 \frac{1}{k_z} \int dv_x \int dv_y \; f(x,y,v_x,v_y,v_z)\Big|_{v_z = U_o = \frac{\omega - \omega_o}{k_z}} .$$

This is exactly the expression for the microwave absorption rate calculated based on the quasilinear theory.

REFERENCES

1. R. A. Dandl, et al., "The ELMO Bumpy Torus Experiment," ORNL/TM-3694, Oak Ridge National Laboratory (November 1971).

2. R. A. Dandl, et al., "Research Program for Plasma Confinement and Heating in ELMO Bumpy Torus Devices," ORNL/TM-4941, Oak Ridge National Laboratory (June 1975).

3. R. A. Dandl, et al., in Proceedings of the Fifth International Conference on Plasma Physics and Controlled Nuclear Fusion Research, Tokyo, Japan, 1974 (IAEA, Vienna, Austria, 1975), Vol. II, p. 141.

4. EBT Experimental Group, "Summary of EBT-1 Experimental Results," ORNL/TM-6457, Oak Ridge National Laboratory (1978).

5. R. A. Dandl, et al., "The EBT-II Conceptual Design Study," ORNL/TM-5955, Oak Ridge National Laboratory (September 1978).

6. G. E. Guest, C. L. Hedrick, and D. B. Nelson, "On the Interchange Stability of a Guiding Center Plasma in an Axisymmetric Mirror Trap," ORNL/TM-4077, Oak Ridge National Laboratory (December 1972).

7. G. E. Guest, C. L. Hedrick, and D. B. Nelson, Phys. Fluids 19, 871 (1975).

8. R. R. Dominguez and H. L. Berk, Phys. Fluids 21, 827 (1978).

9. E. Ott, B. Hui, and K. R. Chu, Phys. Fluids 23, 1031 (1980).

10. D. B. Batchelor and R. C. Goldfinger, Oak Ridge National Laboratory Report ORNL/TM-6992, Oak Ridge National Laboratory (September 1979).

11. R. A. Dandl, H. O. Easo, and H. Ikegami, "Electron-Cyclotron Heating of Toroidal Plasma with Emphasis on Results from the ELMO Bumpy Torus (EBT)," ORNL/TM-6703, Oak Ridge National Laboratory (May 1979).

12. V. A. Flyagin, et al., IEEE Trans. MTT-25, 514 (1977).

13. J. L. Hirshfield and V. L. Granatstein, IEEE Trans. MTT-25, 522 (1977).

14. P. Sprangle and A. Drobot, IEEE Trans. MTT-25, 528 (1977).

15. D. B. Nelson and C. L. Hedrick, "Macroscopic Stability and β Limits in the ELMO Bumpy Torus," ORNL/TM-5967, Oak Ridge National Laboratory (December 1977).

16. D. G. McAlees, et al., "The ELMO Bumpy Torus Reactor (EBTR) Reference Design," ORNL/TM-5669, Oak Ridge National Laboratory (November 1976).

17. S. K. Borowski, N. A. Uckan, E. F. Jaeger, and T. Kammash, Oak Ridge National Laboratory Report #ORNL/TM-6910 (1979).

18. R. J. Kashuba and W. B. Ard, in "EBT Ring Physics, Proceedings of the Workshop," Oak Ridge, Tennessee, p. 333 (December 3-5, 1979).

19. T. H. Stix, Nuclear Fusion 15, 737 (1975).

20. C. F. Kennel and F. Engelmann, Phys. Fluids 9, 2377 (1976).

21. D. Rose and M. Clark, Jr., Plasmas and Controlled Fusion, M.I.T. Press, Cambridge, MA, p. 251 (1961).

22. J. Dawson, "Alternate Concepts in Controlled Fusion," EPRI ER-429-SR, Electric Power Research Institute (May 1977).

23. D. Mosher, Phys. Fluids 18, 846 (1975).

24. T. H. Stix, The Theory of Plasma Waves, McGraw-Hill, New York (1962).

25. M. Fujiwara, et al., in "EBT Ring Physics, Proceedings of the Workshop," Oak Ridge, Tennessee, p. 123 (December 3-5, 1979).

26. O. Eldridge, Phys. Fluids 15, 676 (1972).

27. J. Sperling, "Wave Heating Models for Ion-Cyclotron Heating in EBT-S," J510-80-013, JAYCOR, Del Mar, CA, May 1980 (to be published).

28. L. Spitzer, Physics of Fully Ionized Gases, John Wiley & Sons, New York (1962).